SYNTHESIS AND CHARACTERIZATION OF $LaFeO_3$ USING HIGH ENERGY BALL MILLING

A THESIS SUBMITTED IN THE PARTIAL FULFILLMENT OF REQUIREMENT FOR THE AWARD OF THE DEGREE OF

MASTER OF TECHNOLOGY

IN

MATERIALS SCIENCE AND METALLURGICAL ENGINEERING

SUBMITTED BY

ARVIND KUMAR

ROLL NO. 600902003

SCHOOL OF PHYSICS AND MATERIALS SCIENCE

THAPAR UNIVERSITY, PATIALA–147004

(INDIA)

JULY 2011

DEDICATED TO MY PARENTS AND WELL WISHERS

CERTIFICATE

I hereby declare that the report entitled **"SYNTHESIS AND CHARACTERIZATION OF $LaFeO_3$ USING HIGH ENERGY BALL MILLING"** is an authentic record of my own work carried out as partial fulfillment of the requirements for the award of degree of M.Tech (Materials Science and Metallurgical Engineering) at Thapar University, Patiala, under the guidance of Dr. Puneet Sharma (Assistant Professor) during January to July 2011.

Date: 15-7-2011

Arvind Kumar
(Arvind Kumar)

Roll No. – 600902003

It is certified that the above statement made by the candidate is correct to best of my knowledge and belief.

Dr. Puneet Sharma
Assistant Professor
School of Physics and Materials Science
Thapar University
Patiala -147004

Counter singed by

Dr. O.P. Pandey
Professor and Head
School of Physics and Material Science
Thapar University,
Patiala-147004

Dr. S.K. Mohapatra
Dean of Academic Affairs
Thapar University
Patiala-147004

ACKNOWLEDGEMENT

I would like to express my deepest gratitude to my supervisor Dr. Puneet Sharma for the inspiring guidance, support, encouragement and time commitment during this thesis work. I could not finish my study without his help and encouragement. I believe what I have learnt from him would greatly benefit my future career.

I wish to express my sincere thanks to Dr. O.P. Panday, Professor and Head, School of Physics and Materials Science for permitting and providing the necessary facilities for carrying out thesis.

I am highly grateful to Professor K. K. Raina, Professor N.K Verma, Dr. Kulvir Singh, Dr. D.P. Singh, Dr. S.D. Tiwari and Dr.Bhupendra kumar Chudasama, School of Physics & Material Science, for their kind help and valuable suggestions and special attention throughout my work. It is due to their moral encouragement, love and providing me fountain of inspiration all sorts of assistance from time to time into up-bringing me up to this stage.

I am highly thankful to all Ph.D. Scholar's Mr. Ravi Shukla, Mr.Gurmeet Singh Lotey Mr. Paramjyot Kumar Jha, Mr. Ranvir Singh Panwar, Shiwani Sharma, and Shamiksha Verma of the department for providing all kind of support for carrying out the work.

I would like to give my sincere thanks to Mr. Purushotam Kumar Singh (Lab. Superintendent) for carrying out sample characterization and also thankful to Mr. Jant Singh for his technical assistance.

I am deeply thankful to my family, their moral support and patience has borne fruit through completion of this thesis which will result in award of the prestigious degree of M.tech in Material Science & Metallurgical Engineering.

(ARVIND KUMAR)

CONTENTS

ABSTRACT

In the Present work, lanthanum orthoferrite, $LaFeO_3$ has been prepared using high energy ball milling (HEBM) of La_2O_3 and Fe_2O_3 oxide followed by thermal treatment. Prior to the ball milling, thermal studies of as mixed powder were carried out. The DTA study showed a three endotherm at 344°C, 495°C, and 680°C which is supported by weight loss from TGA. Further the as-mixed powder was milled for different duration, from 3 to 30 hours and heat treated at different temperature. The phase formation studies were carried out in the milled powders and heat treated powders. It was observed the phase formation temperature is about 1200 °C for unmilled samples. However, for milled samples, the phase formation takes place and much lower temperature irrespective to the milling time. A single phase $LaFeO_3$ was obtained at 800°C for all milled samples. The Morphological study of $LaFeO_3$, using SEM, reveals that the particles posses spherical symmetry with well uniformity. The average grain size of is found to be about 200nm. Moreover formation of clusters and aggregation also take place. The room temperature dielectric properties of pure $LaFeO_3$ were measured in the frequency range from 20 Hz to 1MHz using LCR meter. It was found that the value of dielectric constant was high at lower frequency and decrease as the frequency increased and become almost constant at higher frequency region. The dielectric loss was found to be maximum at lower frequency.

LIST OF FIGURES

LIST OF TABLES

CHAPTER - 1

INTRODUCTION

1.1 Perovskite Structure

The mineral "Perovskite" was discovered and named by Gustav Rose in 1839 from samples found in the Ural Mountains, named after a Russian mineralogist, Count Lev Aleksevich von Perovski. The original compound found was calcium titanium oxide ($CaTiO_3$). The name later was used to describe a general group of oxides possessing similar structures with a general formula of ABO_3. In some cases even non-oxides with similar structure are labelled perovskite. Compared to other oxide families such as pyrochlore, perovskite-related compounds can be synthesized with an extremely wide variety of combinations of chemical elements due to several reasons:

1. The perovskite structure accommodates both large (A-site) and small (B-site) cations.
2. Distortions of the ideal cubic structure provide further flexibility for incorporating cations of different sizes
3. The structure is remarkably tolerant of vacancy formation and atomic-scale intergrowths with other structural motifs.

In the ABO_3 perovskite structure A-site can be either M^{+} (Na, K, etc.), M^{2+} (Ca, Sr, Ba, etc.), or M^{3+} (La, Fe, etc.) and the B-site can be occupied by M^{5+} (Nb, W, etc.), M^{4+} (Ce, Ti, etc.), or M^{3+} (Mn, Fe, etc.). The resulting materials can be insulators (as most perovskites have high electrical resistivity), semiconductors, superconductors and ionic conductors.
The ions occupying the A and B lattice sites are detailed in Figure 1.1

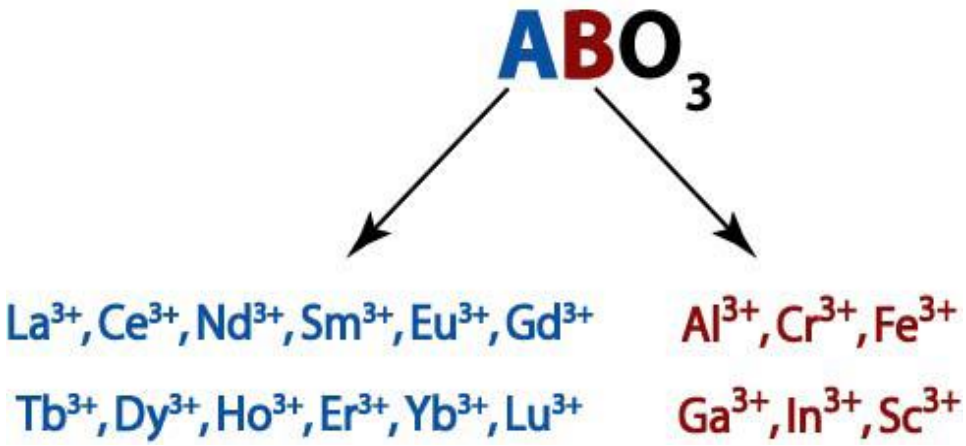

Figure 1.1: Schematic of compositions ABO_3.

The traditional view of the perovskite lattice is that it consists of small B cations within oxygen octahedra, and larger A cations which are XII fold coordinated by oxygen. This structural family is named after the mineral $CaTiO_3$ which exhibits an orthorhombic structure with space group Pnma [100,101]. For the $A^{3+}B^{3+}O_3$ perovskites the most symmetric structure observed is rhombohedral $R\bar{3}c$ (e.g. $LaAlO_3$) which involves a rotation of the BO_6 octahedra with respect to the cubic structure. However, this distortion from the perfect cubic symmetry is slight [100].

1.1.1 Ideal Cubic Structure

The ideal perovskite structure is cubic. The B cations are located in the corners of the cube and the A cation occupies the centre of the cube. The anions are located at the cube edges, between two B cations. Each B cation is surrounded by six anions and forms the centre of the BX_6 octahedra. The BX_6 octahedras extend infinitely in three dimensions. The structure of an ideal cubic perovskite is shown in Figure 1.2 [1, 2]. The perovskite structure can also be regarded as a superstructure of the ReO_3-type that has, in addition, the A cations occupying the cavities (Fig. 1.2 b).

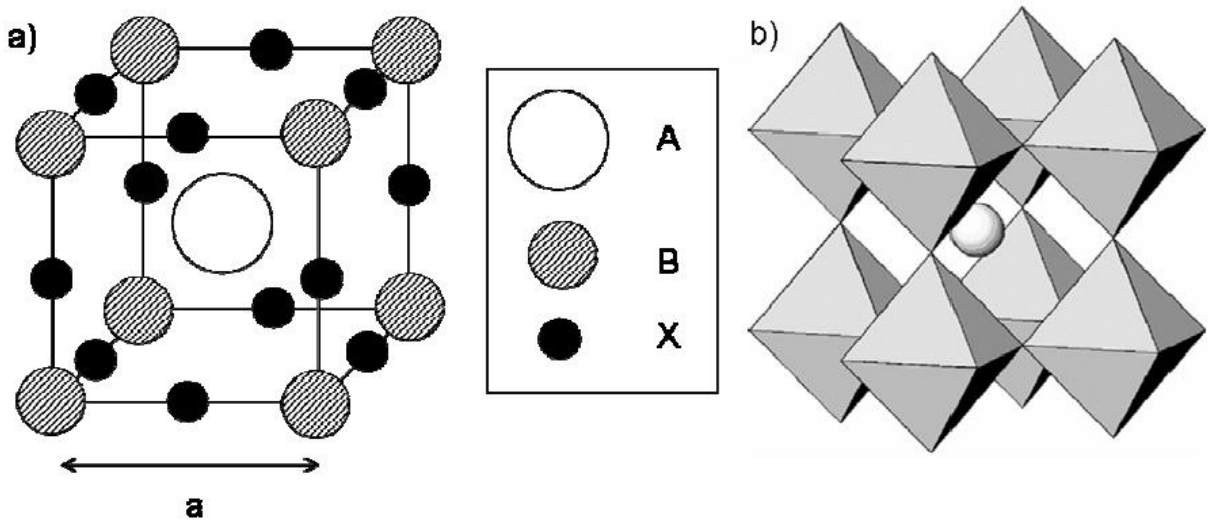

Fig. 1.2 The ideal cubic perovskite structure.

1.1.2 Tolerance Factor

In the ideal perovskite structure, the B-X distance, r_{B-X}, is equal to a/2 and the A-O distance, r_{A-X}, is equal to $a/\sqrt{2}$ where a is a cubic unit cell parameter (Fig. 1.2 a). A useful parameter, *t*, can be defined by the ratio between A-X and B-X distances [1]

$$t = \frac{r_{A-X}}{\sqrt{2}\, r_{B-X}} = \frac{r_A + r_X}{\sqrt{2}\,(r_B + r_X)}$$

Where r_A, r_B and r_X are the respective effective ionic radii. 'T' is the Goldschmidt tolerance factor. [3] The ideal cubic perovskite structure has $t = 1$. It was observed, however, that the perovskite structure remains preserved also when *t* is smaller or larger than 1, in fact $0.75 < t < 1.05$. [4] Nevertheless, the structure becomes distorted and less symmetric. The reduction in symmetry is driven by the necessity to accommodate the anion coordination number around the cations. One or more of the following processes usually happen: [5, 6, 7]

1. Titling of the anion octahedra
2. Displacement of the cations
3. Distortion of the octahedral

These structural distortions were studied in detail by Glazer in 1970s. [5, 6] Glazer provided a classification of lattice distortions of perovskites and described 23 different tilt systems. [5]

1.2 Pervoskites Material Properties

Perovskite materials exhibit many interesting and intriguing properties from both the theoretical and the application point of view. Colossal magneto resistance, ferroelectricity, superconductivity, charge ordering, spin dependent transport, high thermo power and the interplay of structural, magnetic and transport properties are commonly observed features in this family. These compounds are used as sensors and catalyst electrodes in certain types of fuel cells and are candidates for memory devices and spintronics applications.[8]

Many superconducting ceramic materials (the high temperature superconductors) have perovskite-like structures, often with 3 or more metals including copper, and some oxygen positions left vacant. One prime example is yttrium barium copper oxide which can be insulating or superconducting depending on the oxygen content.

Chemical engineers are considering this material as a replacement for platinum in catalytic converters in diesel vehicles.[9]

1.3 Perovskites Applications

Perovskites find technical application in ceramics, refractories, and electronics, as well as possible hosts for nuclear waste. Table 1.1 lists the properties and applications of some commonly investigated perovskites.

Table 1.1 Properties and applications of some perovskites

Property	Application	Compound
Optical property	Electro optical modulator, laser host, switch, second harmonic generator	(Pb,La)(Zr,Ti)O_3, YAlO3,$LiNbO_3$, $KNbO_3$
Ferroelectric/pie-zoelectric	Piezoelectric transducer, P.T.C.thermistor, electrostrictive actuator	$BaTiO_3$, Pb(Zr,Ti)O_3, Pb(Mg,Nb)O_3
Magnetic property	Magnetic bubble memory, ferromagnet	$GdFeO_3$, $LaMnO_3$
Electrical and Dielectric Property	Multilayer capacitor, dielectric resonator, thin film resistor	$BaTiO_3$, $BaZrO_3$
Ionic conducting	Solid electrolyte	(La,Sr)(Ga,Mg)$O_{3-\delta}$
Proton conducting	SOFC electrolyte hydrogen sensor	$BaCeO_3$, $SrCeO_3$, $SrZrO_3$, (La,Sr)$MnO_{3-\delta}$
Mixed conducting	SOFC electrode	$BaPrO_3$, $LaCoO_3$
Super conducting	superconductor	Ba(Pb,Bi)O_3
Catalytic property	catalyst	$LaFeO_3$, La(Ce,Co)O_3

1.4 Lanthanum Orthoferrite, $LaFeO_3$

$AFeO_3$ oxides (the so-called orthoferrites) belong to a relevant class of weak ferromagnetic materials with interesting magnetic and magneto-optical properties [10,11]. The magnetic structure in orthoferrites can be conventionally described by two interpenetrating pseudo-cubic face centred sub-lattices in which each Fe^{3+} ion is surrounded by six O^{2-} ions. This results in a collinear arrangement of the two sub-lattices, giving an antiferromagnetic ordering. However, the FeO_6 octahedra can be tilted to different degrees depending on the size of the rare-earth cation, leading to a net magnetic moment [12,13]

Lanthanum orthoferrite, $LaFeO_3$, is one of the most common perovskite-type oxides and has an orthorhombic perovskite structure with space group Pbnm. $LaFeO_3$ consists of FeO_6 octahedra units with La^{3+} ions inserted between these units. Bulk $LaFeO_3$ is known to be antiferromagnet with a Neel temperature T_N of 740 °C [14]. It has much practical interest for electroceramic applications due to their attractive mixed conductivity displaying ionic and electronic defects. The mixed ionic-electronic conductivity of $LaFeO_3$ exhibits a linear response to oxygen pressure and provides oxygen sensor applications [15]. The excellent sensitivity and selectivity towards various toxic gases such as CO and NOx are observed as well [16]. Moreover, $LaFeO_3$ nanoparticles exhibited good photocatalytic properties under visible light irradiation [17, 18]. These properties are enhanced by the homogeneity and high surface area of the fabricated $LaFeO_3$ particles. Fine particles with diameter of less than 100 nm are potentially required for these purposes. its spontaneous magnetization is considerably small, 0.044 μB/Fe [19]. However, antiferromagnetic nanoparticles often exhibit increasing net magnetization due to the presence of uncompensated surface spins [20, 21]. If the ferromagnetic behaviour is promoted in $LaFeO_3$, it should provide facile handling of their applications by using magnetic field.

Conventionally solid-state oxide reaction method was used for preparation of $LaFeO_3$. This conventional route is employed due to simplicity and low manufacturing cost. The method results in single phase of perovskite. However, it is associated with drawbacks such as diffusional constrain to synthesis results into slow kinetics and high temperatures results in uncontrolled particle size and lower surface area. Alternative routes to solid-state reaction method are wet chemical synthesis methods such as, co-precipitation, combustion, sol–gel methods, etc. [22,23]. In all these wet chemical synthesis methods, pure phase formation can be accelerated, as it involves mixing of elements at atomic level and lower calcinations temperatures. In addition to this, it is possible to have controlled particle size, morphology, and improvement in surface area. Based on the good applications different synthesis methods have been used by different researchers **.** A number of attempts have been made for synthesis of $LaFeO_3$ for different purposes. For example, co- precipitation method was used for synthesis of $LaFeO_3$, nanocrystaline $LaFeO_3$ perovskite with particle size of 59nm was synthesized by Wang et al. by using combustion method. Solution combustion synthesis , sol–gel , sol–gel auto combustion hydrothermal synthesis [24], polymerisable complex [25], Cui et al. used sol–gel method for the same [26] and low temperature thermal decomposition. In all these methods final calcinations temperature was in range of 500°C–950 °C.

1.5 Structure of $LaFeO_3$

$LaFeO_3$ first in the series of rare earth orthoferrites, exhibits like all of its members, an orthorhombically distorted perovskite structure with space group Pbnm [27,28]. The atomic positions in the unit cell have been determined by X-ray diffraction on small twinned single crystals [29]. In this structure Fe^{3+} ions are located at the centers of slightly distorted O^{2-} octahedral. The Fe^{3+} ions are coupled antiferromagnetically to six Fe^{3+} nearest neighbours via Fe-O-Fe super exchange and exhibit G-type antiferromagnetic ordering like all the other rare earth perovskites [30, 31]. It has been assumed that the magnetic moments point along the crystallographic a-direction because such is the case with all the other members of the series at high temperatures.

Lanthanum ferrite, $LaFeO_3$, crystallises in the orthorhombic space group Pbnm at temperatures below ~ 1273 K. [27] At temperatures above 1273 K, it has a rhombohedral structure with space group $R\bar{3}c$.[32] The crystal structure of $LaFeO_3$ is shown in Fig. 1.3

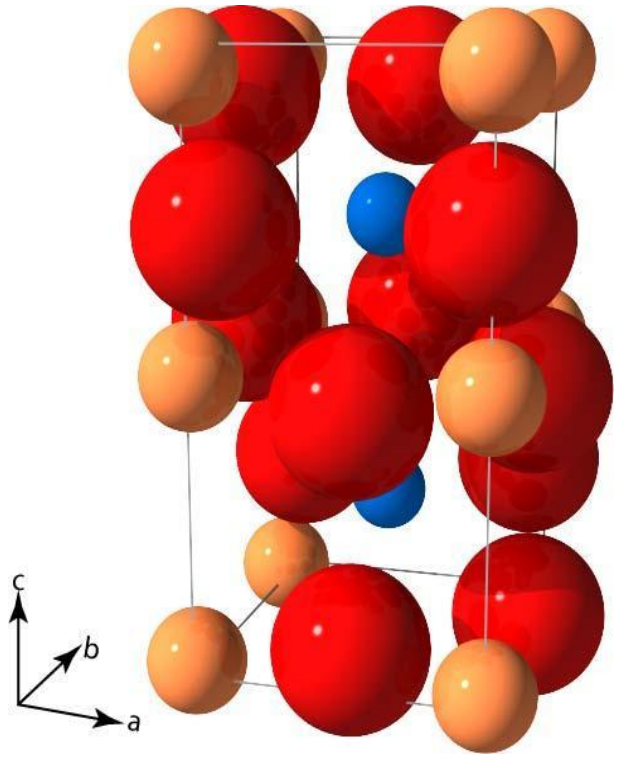

Figure 1.3 : Pbnm, orthorhombic perovskite unit cell. Blue, yellow, red respectively A cations, B cations, oxygen ions

1.6 Phase diagram of $LaFeO_3$

Pure $LaFeO_3$ have a very narrow homogeneity range. It becomes oxygen deficient at a significantly lower oxygen partial pressure compared to $LaCoO_3$. The phase diagram of the pseudo-binary La_2O_3 – Fe_2O_3 system is given in Fig.1.4 [33]. Beside the $LaFeO_3$ phase, only one other ternary compound was found, $LaFe_{12}O_{19}$. This phase is ferromagnetic and 1/12 of the iron is in the ferrous state. The $LaFe_{12}O_{19}$ phase decomposes to $LaFeO_3$ and Fe_3O_4 at 1694 K.

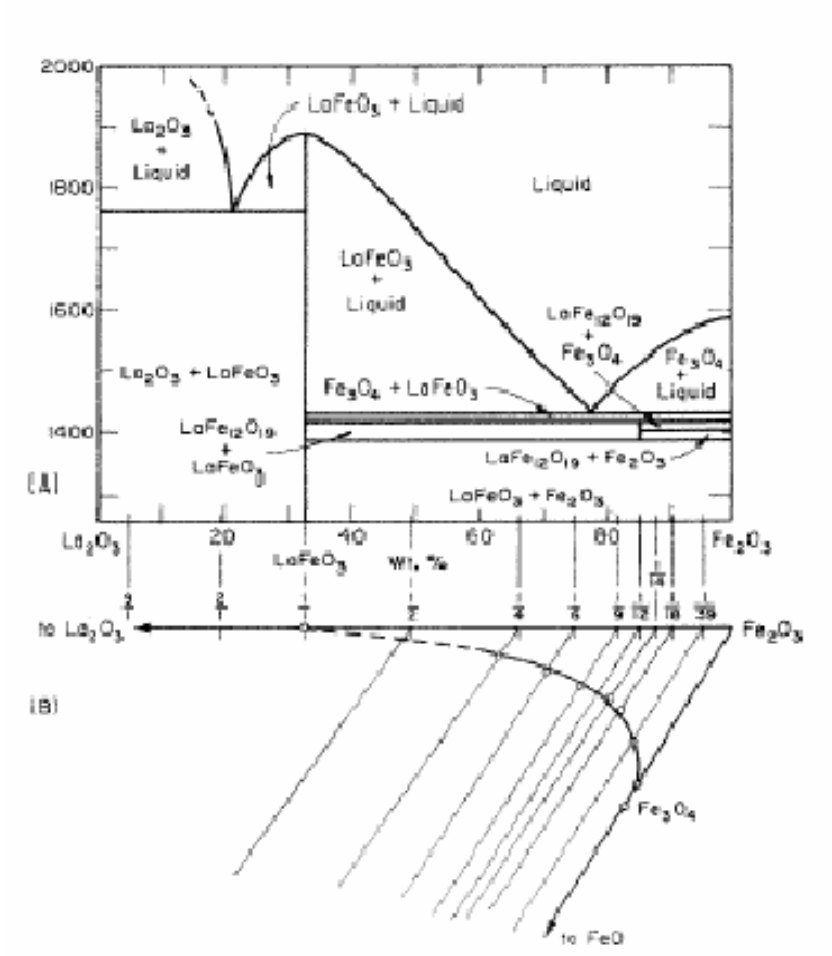

Fig. 1.4. Phase diagram of the $LaFeO_3$ - La_2O_3 & Fe_2O_3 system in air. Temperature is given in °C.

1.7 Synthesis of $LaFeO_3$ by Different Route

$LaFeO_3$ is synthesized by many methods. There are various type of method to process $LaFeO_3$ which can classify in major four types:

[1] Co-precipitation Method

[2] Combustion Method

[3] Sol–gel Method

[4] High energy ball milling

1.7.1 Co-precipitation method

In the co-precipitation method, aqueous solutions of lanthanum nitrate and iron nitrate were prepared separately and mixed together in 1:1 molar ratio. The prepared solution was dropped slowly into 50% ammonia solution (i.e. 0.08 mol $L^{-}1$ ammonia concentrations) to form precipitate. After complete precipitation, the resultant brown precipitate was aged for 24 h. Subsequently precipitate was dried at 120°C for 12 h. In order to prepare crystalline $LaFeO_3$ perovskite dried precursor was subjected to calcinations by using a predefined heating cycle as depicted in Fig. 1.5 This specific heating cycle, with relatively slow heating rates and long holds at temperatures, is important in phase formation of perovskite with retaining higher surface area.

The reactions for co-precipitation method could be described as given below

$$La(NO_3)_3 + Fe(NO_3)_3 + NH_4OH \rightarrow La(OH)_3 + Fe(OH)_3 + NH_4NO_3$$

$$La(OH)_3 + Fe(OH)_3 \rightarrow LaFeO_3$$

According to reactions given above, nitrates are precipitated in the form of hydroxides, respective hydroxides undergo reaction, and yields required perovskite product.

1.7.2 Combustion method

In this technique, the stoichiometric amount of $La(NO_3)_3 \cdot 6[H_2O]$ and $Fe(NO_3) \cdot 9[H_2O]$ were mixed together in aqueous medium with glycine solution (H_2NCH_2 COOH). Glycine to total metal ion molar concentration ratio was two. The solution was ignited by rapidly heating up to 200 °C; on ignition, vigorous fumes of CO_2 and nitrogen were formed. The ignition raises the local temperature, which helps in formation of perovskite,

even though provided temperature was lower. Resulting product consist of mixed oxide phases and needs further calcinations to synthesis targeted product [34].

The calcination of resulting product oxide was carried out using a defined heating cycle as in Fig 1.5 The temperature was raised from room temperature to 800 ˚C within 2 h with heating rate of 5 ˚Cmin¯1 and holding it at 800 ˚C for 4 h.

The reaction for combustion method is as follows [35]:

$$La(NO_3)_3 + Fe(NO_3) + 3.3H_2N(CH_2)CO_2H + 7.5O_2 \rightarrow LaFeO_3 + 6.67CO_2 + 7.5H_2O + 1.67N_2$$

1.7.3 Sol–gel method

The pure phase $LaFeO_3$ perovskite was prepared by employing the sol–gel (Pechini) method. Lanthanum nitrate hexahydrate and iron nitrate nonahydrate was dissolved in distilled water. Metal ions present in resulting aqueous solution undergo complexation by adding 1mol of citric acid per mole of metal ions. The resulting sol was heated at 70–80 ˚C (using 2 ˚Cmin¯1 heating rate) in order to induce the gel formation. Prepared gel consisting of metal citrate complex was subjected to calcination [36].

Calcinations of citrate a precursor was carried out using a cycle which involves raising the temperature from room temperature to 600 ˚C within 2 h hold on the same for 2 h. Further, the temperature was raised to 800 ˚C and held for 4 h.

The reaction for sol–gel method is as follows [37]:

$$La(NO_3)_3 \cdot 6H_2O + Fe(NO_3)_3 \cdot 9H_2O + C_6H_8O_7 \cdot H_2O \rightarrow LaFeO_3 + 6CO_2 + 3N_2 + nH_2O$$

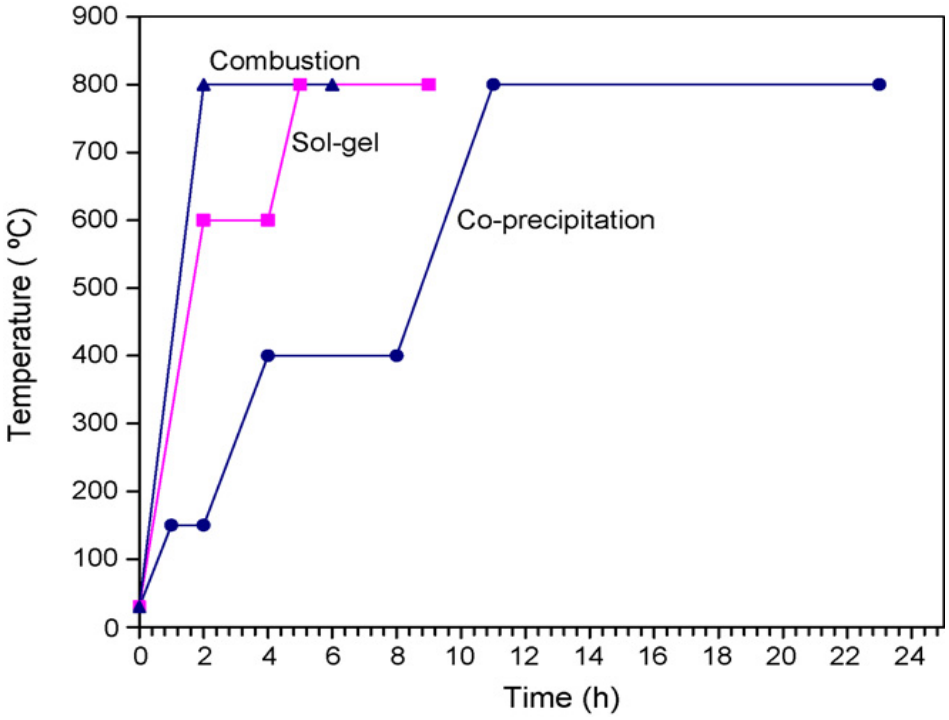

Fig. 1.5 Heating cycle used for calcinations in various methods.

1.7.4 High Energy Ball Milling (HEBM)

Ball mill is a good tool for grinding many materials into fine powder. The Ball Mill is used to grind many kinds of mine and other materials. There are two type of grinding: the dry process and the wet process. It can be divided into tabular type and flowing type according to different forms of discharging material. After the grinding the state of the solid is changed: the size and shape of grain etc.

The ball mill is key equipment for grinding. It is widely used for the cement, the silicate product, new type building material, fire-proof material, chemical fertilizer, black and non-ferrous metal, glass, ceramics and etc. Ball mill can grind ore or other materials that can be grinded either by wet process or by dry process. Benefits of high energy ball milling are following:

- Increase of the surface area of a solid
- Manufacturing of a solid with a desired grain size
- Pulping of resources

1.8 Applications of $LaFeO_3$

Metal oxides and perovskites are being employed as catalysts for various applications [38].$LaFeO_3$ is one of the important perovskite widely reported for various applications including

1. Solid oxide fuel cells
2. Sensors
3. Oxygen permeation membranes.
4. As environmental catalyst

CHAPTER - 2

LITRETURE REVIEW

In this chapter the important work carried out in last few years related to synthesis of $LaFeO_3$ by different method and the substitution effect on the properties has been reviewed.

T. Peterlin-Neumaier *et al.* 1986[39] resolved for the first time the diffraction peaks (101) and (011) of $LaFeO_3$, arising from the extremely small orthorhombic distortion ***(***b/a = 1.002). The intensity ratio *R* = I(011)/I(101) = 2.32± 0.12 indicated a clear deviation from a pure G_x, antiferromagnetic configuration of Fe^{3+} ions requiring *R* = 3. Refinement of the entire measured spectrum from the powder specimen, taking the increasingly important secondary extinction into account, showed that the magnetic moments are tilted with respect to the crystallographic a-axis. Two limiting values for their orientation could be determined given by the tilt angle $\alpha = 18.2^{\circ} \pm 6.4^{\circ}$ in the ac-plane (G_{xz}) and $\alpha = 11.7^{\circ} \pm 6.6^{\circ}$ in the ab-plane (G_{xy}). Due to the excellent resolution of the TOF diffractometer they were able to resolve diffraction lines arising from the extremely small orthorhombic deformation of $LaFe0_3$ in the ab-plane. From the intensity ratio of the two most important antiferromagnetic lines (101) and (011) which have been here resolved for the first time, they obtained a preliminary idea of the magnetic moment direction. The application of Rietveld profile refinement to the entire measured spectrum furnished more precise values of the spin orientation. They showed a mixing of at least two modes rather than a simple G_x antiferromagnetic arrangement of Fe^{3+} moments. Since this is not permitted by symmetry considerations. Crystal symmetry must be lower. i.e. $LaFeO_3$, should exhibit monoclinic rather than orthorhombic structure.

Kuiying Li *et al.* 1999[40] studied the effects of surface and quantum confinement on nano-$LaFeO_3$ surface adsorbed by the sensor gas, probed by vacuum adsorptive surface photo voltage technique. The quantum confinement effect depends exponentially on the pressure of the sensor gas. There are two main ways of charge transfer transition on the adsorbed nano-$LaFeO_3$ surface. By the surface photo voltage vs. the light wavelength under d.c. electric field induction and exposure of the samples to the sensor gas, it turns out that nano- $LaFeO_3$ shows a very different electric conduction character compared with the conventional crystalline

$LaFeO_3$ because of the surface effects of nanomaterial. In addition, nano- $LaFeO_3$ surface adsorbed by ethanol molecules exists in two different ways of charge transfer transition.

Qiwu Zhang *et al.* 2001[41] synthesized mechanochemically $LaFeO_3$ by room temperature grinding of La_2O_3 and Fe_2O_3 powders when the Fe_2O_3 sample with crystallite size less than 20 nm is used. Fe_2O_3 powder with smaller crystallite size obtained by heating at lower temperature reacts more easily with La_2O_3 than that with larger size. The mechanochemical reaction proceeds with an increase in grinding time. Specific surface area of the $LaFeO_3$ powder synthesized has a large value of over 11 m^2/g. The mechanochemical process can be also applied to synthesize other iron complex oxides with rare earth elements such as Pr, Nd and Sm. $LaFeO_3$ powder can be simply This solid reaction tends to be difficult with the increase in crystallite size of Fe_2O_3 powder. The obtained $LaFeO_3$ powder sample consists of agglomerates with fine grains of nanometer size.

S. Nakayama *et al.* 2001[42] synthesized the perovskite oxide, $LaFeO_3$, by three different preparation methods i.e., the calcinations of a mixture of La_2O_3 and Fe_2O_3 (La-Fe-O), a co-precipitated precursor (La-Fe-OH), $La(OH)_3$ and $Fe(OH)_3$, and a heteronuclear complex (La-Fe-CN), $La[Fe(CN)_6]$ $5H_2O$. The obtained powders were characterized by thermogravimetric analysis, powder X-ray diffraction, electron microprobe analysis, specific surface area measurement and scanning electron microscopy. The formation of $LaFeO_3$ is clearly recognized for La-Fe-O, La-Fe-OH and La-Fe-CN at calcining temperatures above 1000, 800 and 600◦C, respectively. The mean particle diameter of La-Fe-CN calcined at 600°C for 2 hours was 30 nm. The $LaFeO_3$ perovskite oxide powder obtained by the thermal decomposition of La-Fe-CN was most uniform on an atomic level and the nanosized $LaFeO_3$ powder was obtained at low temperatures. Furthermore, the sinterability was good. The estimated activation energy for the crystal growth of the $LaFeO_3$ perovskite oxide decreased in the order of La-Fe-O> La-Fe-OH>La-Fe-CN. Furthermore, the sinterabilities at 1300◦C increased in the order of La-Fe-O<<La-Fe-OH<La-Fe-CN. Based on these results, it is found that the $LaFeO_3$ perovskite oxide powder synthesized by the thermal decomposition of the La $[Fe(CN)_6]$. $5H_2O$ hetronuclear complex is the most uniform on an atomic level and the formation of pure and the nanosized $LaFeO_3$ powder is obtained at low temperatures.

A. Delmastro *et al.* 2001[43] Synthesized $La_{(1-\varepsilon)}FeO_{(3-1.5\varepsilon)}$ perovskite catalysts (ε=0, 0.1, 0.2, 0.3) by low-temperature thermal decomposition of La and Fe nitrates and further heating to 873 K in air. They are characterized by DTA, XRD, BET, SEM, Mossbauer spectroscopy

and tested for the catalytic combustion of methane. All oxides are monophasic; for ε=0 the structure is orthorhombic, whereas for $0<\varepsilon\leq0.3$ a pseudo cubic symmetry is evident. The Mossbauer spectra are characterized by antiferromagnetic sextuplets; for ε=0.3 a doublet is also present. The catalytic activity toward CH_4 oxidation appears to be strongly enhanced in the samples with ε>0; the most active composition corresponds to ε=0.1, while for ε=0.2 and 0.3 the catalytic activity is slightly decreased. The results are explained assuming that the excess of iron oxide in the ε>0 samples corresponds to the presence of surface of layers of FeO_5 polyhedra, coordinatively unsaturated, according to proposed structural model.

Monica Popa *et al.* 2002[44] Successfully synthesized powders of $LaFeO_{3+d}$ by a simple technique polymerizable complex route based on polyesterification reaction between CA and EG i.e. a mixed solution of citric acid (CA) and ethylene glycol (EG) with La and Fe ions was polymerized. X-ray diffraction results indicated the formation of perovskite-type, which crystallizes in orthorhombic system $LaFeO_{3+d}$ when the La–Fe polymeric precursor was treated at 550 ^{0}C for 6 h. A good mixing and a good distribution of cations in the solutions were achieved by PC method, which assures a good chemical and compositional homogeneity in the powder precursor. The advantages offered by PC route for obtaining powders of $LaFeO_{3+d}$ are the low crystallization temperature of a single-phase material compared to other methods, the simplicity of the method and the homogenous microstructure of the powder obtained.. The formation mechanism, the homogeneity, and the structure of the obtained powders have been investigated by thermogravimetry, X-ray diffraction, Raman spectroscopy, and scanning electron microscopy (SEM) measurements.

M. Sivakumar *et al.* 2003[45] prepared nanocrystalline perovskite-type $LaFeO_3$ with particle size of about 30 nm by a sonochemical method using iron pentacarbonyl and lanthanum carbonate as starting materials. The overall process involves three steps: formation of lanthanum carbonate using lanthanum nitrate and urea; reaction of the so-formed lanthanum carbonate with iron pentacarbonyl resulting in the formation of a precursor; calcination of the precursor to obtain nanocrystalline particles of $LaFeO_3$. Transmission electron microscopy revealed the particles to have a mean size of about 30 nm. Study of the magnetic properties of nanocrystalline $LaFeO_3$ particles shows a coercivity of ~250 Oe, while the saturation magnetization is ~40 memu g^{-1}. The obtained nanoferrite powder is expected to be used in applications for functional ceramics (sensors, SOFCs, electrodes, or even magnetic and ferroelectric applications).

Xiwei Qi *et al*. 2003[46] prepared nanosized $LaFeO_3$ powders of 30 nm particle size by sol-gel auto-combustion at room temperature. The overall process involves three steps: formation of homogeneous sol; formation of dried gel; and combustion of the dried gel. Experiments revealed that $LaFeO_3$ dried gel derived from citrate and nitrate sol exhibits self-propagating combustion at room temperature once it is ignited in air. After auto-combustion, the gel directly transforms into nanosized $LaFeO_3$ particles. The auto combustion was considered as a heat-induced exothermic oxidation–reduction reaction between nitrate ions and carboxyl group. Differential thermal analysis–thermogravimetry (DTA–TG) was used to study the decomposition of the precursor. The structure of the nanosized $LaFeO_3$ powders was characterized by X-ray diffraction (XRD).

A. Fossdal *et al.* 2005[47] reported the fracture strength, fracture toughness and apparent Young's modulus of $LaFeO_3$ ceramics in the temperature region 25–800 °C. The fracture strength of the material was observed to increase from 202 ± 18MPa at room temperature to 235 ± 38MPa at 800°C. The room temperature fracture toughness was 2.5 ± 0.1MPa $m^{1/2}$. The fracture toughness decreased to 2.1 ± 0.1 MPa $m^{1/2}$ at 600 ◦C, followed by an increase to 3.1 ± 0.3MPa $m^{1/2}$ at 800 ◦C. The temperature dependence of the fracture toughness correlates well with the crystallographic strain, $|(a - c)|/(a + c)$, and ferroelastic toughening of $LaFeO_3$ materials is inferred. Ferroelastic behaviour of $LaFeO_3$ ceramics is demonstrated by a partial hysteresis loop measured under cyclic compression. The coercive stress is in the order of 20MPa, and the residual strain after application of a stress of 500MPa is 0.025%. Ferroelastic toughening was observed, and the variation in fracture toughness with temperature correlates with the magnitude of the crystallographic strain. The promising mechanical properties make $LaFeO_3$ a potential candidate as a load-bearing material in high-temperature devices.

Ivar Waernhus *et al.* 2005[48] reported the electrical conductivity of polycrystalline $LaFeO_3$ as a function of temperature and prepared $LaFeO_3$ and $La_{0.99}Sr_{0.01}FeO_3$ ceramic powder by a combination of spray drying and glycine/ nitrate combustion. The conductivity of $LaFeO_3$ was shown to be affected by annealing for extended periods (about one week) at temperatures above 1000^0C prior to the conductivity measurements. Higher annealing temperatures resulted in higher conductivity. This effect was explained by the formation of Schottky cation defects, which act as electron acceptors, leading to an increasing conductivity with increasing annealing temperature. Below 1000 ^{0}C, the conductivity was unaffected by the annealing temperature, probably due to the low mobility of cation vacancies. A model for the defect

chemistry and conductivity of $LaFeO_3$, including the formation of Schottky defects is proposed. The model reproduces quantitatively the dependence of the conductivity with respect to the partial pressure of oxygen at 1000 ^{0}C. The electronic mobilities of the charge carriers in the material were determined by the conductivity of $La_{0.99}Sr_{0.01}FeO_3$, where the charge carrier concentration is given by the dopant level. The model also predicts that the concentration of p-type charge carriers in air is increasing with temperature due to the formation of Schottky defects, for a limited temperature interval above 1000 ^{0}C. The present study has demonstrated that the conductivity of polycrystalline $LaFeO_3$ is dependent on the thermal history. The conductivity is enhanced by annealing the materials above 1000 ^{0}C. This phenomenon is explained by the formation of Schottky defects which acts as electron acceptors. The formation of cation vacancies is rate controlled by cation diffusion, and sufficiently long annealing time is necessary in order to reach an equilibrium vacancy concentration.

M. A. Gabal *et al*. 2006[49] synthesized the oxalate mixture $La_2(C_2O_4)_3.10H_2O–FeC_2O_4.2H_2O$ (1:2 mole ratio) using the impregnation technique in which few drops of bidistilled water was added to the desired mole ratios of the individual metal oxalates with vigorous stirring then the mixture was dried in a thermostated oven at 50 ^{0}C for 1 h. Pure metal oxalates, $La_2(C_2O_4)_3.10H_2O$ and $FeC_2O_4.2H_2O$ were synthesized by mixing aqueous solutions of stoichiometric amounts of analytical grade $LaCl_3.7H_2O$ or $FeSO_4.7H_2O$ with analytical pure reagent of oxalic acid under continuous stirring. The resulting precipitates were collected by suction filtration and then washed with water, ethanol before drying in a thermo stated oven at about 50^{0}C. Thermal processes involved during the decomposition course of $La_2(C_2O_4)_3.10H_2O–FeC_2O_4.2H_2O$ (1:2 mole ratio) mixture up to 750 ^{0}C, in an atmosphere of air, were monitored by thermogravimetry and differential thermal analysis. X-ray diffraction and Mossbauer spectroscopy were used to characterize the intermediates and the final product. The results showed that a microcrystalline or possibly amorphous iron (III) oxide with a paramagnetic nature was appeared in the early stages of decomposition at 250 ^{0}C. By increasing the temperature, a well crystalline hematite with ferromagnetic properties was obtained. XRD pattern of the mixture calcined at 1100 ^{0}C shows the formation of $LaFeO_3$ single phase in consistent with the hyperfine magnetic splitting (one sextet of lines) characteristic of $LaFeO_3$ obtained in the Mossbauer spectra of the mixture calcined at the same temperature.

G. Shabbir *et al.* 2006[50] developed a novel sol–gel process for preparing nano-sized, perovskite-type $LaFeO_3$ powder by the thermal decomposition of the gel complex of LaFe–($C_6H_8O_7 \cdot H_2O$). The structural evolution has been systematically investigated by X-ray diffraction (XRD), differential thermal analysis (DTA) and thermo gravimetric analysis (TGA). Perovskite powder of ~25 nm size could be obtained at a temperature of ~600 °C without formation of any secondary phases of La_2O_3 and Fe_2O_3 single oxides and no requirements of high temperature/vacuum/pH control etc. By careful control of gelling conditions the formation of $LaFeO_3$ perovskite phase can be achieved without passing through explosion/combustion process and pH control. XRD results confirmed that although the disordered phase of La_2O_3 appeared at ~350 °C but it was transformed completely into the perovskite phase at/above 600 °C with final particle size of the order of ~25 nm.

Yanping Wang *et al.* 2006[51] prepared orthorhombic structure perovskite $LaFeO_3$ nanocrystals with size of 59 nm by glycine combustion method. The as-prepared $LaFeO_3$ nanocrystals were characterized by X-ray diffraction (XRD), transmission electron microscopy (TEM), high reaction transmission electron microscopy (HRTEM), energy dispersive X-ray spectrometer (EDS), scanning electron microscope (SEM), UV–Visible absorption spectroscopy, Laser Raman Spectroscopy (LRS) and Brunauer–Emmett–Teller (BET) nitrogen adsorption. The preparation process can be also applied to synthesize other complex oxides such as $NdFeO_3$, $LaCoO_3$ and $LaNiO_3$.

A.D. Jadhav *et al.* 2007[52] employed a combination of digestion and further low temperature calcination to crystallize the product to prepare $LaFeO_3$ (LF) and $LaCoO_3$ (LC) powders. Freshly co-precipitated lanthanum and ferric (or cobalt) hydroxide gels by sodium hydroxide were allowed to react at 100 °C under refluxing and stirring conditions for 4–6 h. These oven dried powders were heated at 450 °C to form crystalline LF (or LC) powders. The phase contents and lattice parameters were investigated by X-ray diffraction (XRD). Transmission electron microscope (TEM) investigations were carried out to examine the morphology and average particle size of these powders. A simple two steps process is used for the preparation of ultrafine powders of $LaFeO_3$ or $LaCoO_3$ from simple hydroxides precursor. This is the lowest temperature reported so far for the formation of LF (or LC) phase. The average particle size and morphology of these powders were investigated by transmission electron microscopy.

Defne Bayraktar *et al.* 2007[53] produced tubular membranes of $La_{0.6}Ca_{0.4}Fe_{0.75}Co_{0.25}O_{3-\delta}$ and $La_{0.5}Sr_{0.5}Fe_{1-y}Ti_yO_{3-\delta}$ (y = 0, 0.2) for the application of partial oxidation of methane to syngas by thermoplastic extrusion and investigated by oxygen permeation measurements. Thermoplastic feedstocks with different ceramic content were produced and their viscosities measured as a function of the shear rate. About 51 vol.% ceramic content was found to be optimum for tube production. Straight tubes could be obtained with outer diameter of 4.8–5.5mm and thickness of 0.25–0.47 mm. The sintered tubes had more than 95% of theoretical density. The oxygen permeation flux of the tubular membranes was measured with air on one side and Ar or Ar +CH_4 mixture on the other side. The oxygen permeation rate decreased with Ti-substitution while it was considerably increased by introduction of 5% methane into the system. The normalized oxygen fluxes in air/Ar gradient at 900 ˚C were measured to be 0.06, 0.051, and 0.012 µmol cm^{-2} s^{-1} for LCFC, LSF, and LSFT2, respectively, and 0.18 µmol cm^{-2} s^{-1} for LSFT2 with 5% methane. Tubular membranes of $La_{0.6}Ca_{0.4}Fe_{0.75}Co_{0.25}O_{3-\delta}$ and $La_{0.5}Sr_{0.5}Fe_{1-y}Ti_yO_{3-\delta}$ (y = 0, 0.2) were produced by thermoplastic extrusion. The oxygen permeation flux of the tubular membranes were measured in a system where air was introduced through the inner side of the tube and Ar or Ar +CH_4 mixture was introduced in the outer catalytic side, which was covered with a oxide-based catalytic layer. The oxygen fluxes in an air/Ar gradient at 900 ˚C were measured to be 0.24, 0.11, and 0.034 µmol cm^{-2} s^{-1} for LCFC, LSF, and LSFT2, respectively; 0.49µmol cm^{-2} s^{-1} for LSFT2 with 5% methane. The Ti-substitution decreased the oxygen permeation rate. The LCFC shows a superior stability at similar permeation rates allowing operation in pure CH_4 over several hundreds of hours.

Xiaoping Dai *et al.* 2008[54] investigated by continuous flow reaction and sequential redox reaction comparison of LaFeO3, $La_{0.8}Sr_{0.2}FeO_3$, and $La_{0.8}Sr_{0.2}Fe_{0.9}Co_{0.1}O_3$ perovskite oxides as oxygen carrier for partial oxidation of methane in the absence of gaseous oxygen. Methane was oxidized to syngas with high selectivity by oxygen species of perovskite oxides in the absence of gaseous oxygen. The sequential redox reaction revealed that the structural stability and continuous oxygen supply in redox reaction decreased over $La_{0.8}Sr_{0.2}Fe_{0.9}Co_{0.1}O_3$ oxide, while $LaFeO_3$ and $La_{0.8}Sr_{0.2}FeO_3$ exhibited excellent structural stability and continuous oxygen supply. The sequential redox reactions over $LaFeO_3$, $La_{0.8}Sr_{0.2}FeO_3$, and $La_{0.8}Sr_{0.2}Fe_{0.9}Co_{0.1}O_3$ suggest that the catalytic activity of methane oxidation and the amount of oxygen replenished in a reoxidation procedure increases with the replacement of A site with Sr ($La_{0.8}Sr_{0.2}FeO_3$), or with the replacement of the total A and B sites

($La_{0.8}Sr_{0.2}Fe_{0.9}Co_{0.1}O_3$). There is an increase in reactivity and availability of oxygen species, but a decline in CO selectivities with A-site and B-site substitution. The structural stability and continuous oxygen supply in redox reaction decrease over $La_{0.8}Sr_{0.2}Fe_{0.9}Co_{0.1}O_3$ oxide, while $LaFeO_3$ and $La_{0.8}Sr_{0.2}FeO_3$ exhibit excellent structural stability as well as continuous oxygen supply.

L. John Berchmans *et al.* 2008[55] prepared fine crystalline $LaFeO_3$ and antimony-substituted compound by co precipitation method. The as synthesized materials have been sintered at 1000 $^{\circ}$C for single-phase compound formation and evaluated for their electrical and structural properties. TG/DTA studies ascribed that the precursor powders have undergone rapid changes during the transformation of $LaFeO_3$ and substituted compounds. XRD data reveal the presence of well-defined sharp peaks, indicating the single-phase perovskite structure of $LaFeO_3$ and polycrystalline structure of $LaFeO_3$ and Sb_2O_3 compounds. The FT–IR spectra exhibit an absorption band corresponding to Fe–O stretching vibration, which is shifted on the substitution of Sb^{3+} ions. The temperature dependent d.c. conductivity shows the semiconducting behaviour of the synthesized materials. The band gap values are found to increase up to $x = 0.4$ and decrease on further increase in concentrations of the Sb^{3+} ions. The decrease in dielectric constant with increasing frequency explained the Maxwell–Wagner Interfacial polarization model. The electrical conductivity of the synthesized $LaFeO_3$ and substituted compounds are found to increase with increasing measuring temperature. AC electrical conductivity shows that the dielectric constant is found to decrease with increase in frequency. The SEM images reveal the presence of fine crystallites formation of the parent and substituted compounds of $LaFeO_3$.

S. Petrovic *et al.* 2008[56] prepared two new series of perovskite-type oxides $LaMO_3$ (M = Mg, Ti, Fe) with different ratio Mg/Fe (MF) and Ti/Fe (TF) in the B cation site by annealing the precursor, obtained by the mechanochemical activation (MCA) of constituent metal oxides, at 1000 ^{0}C in air. In addition, two closely related perovskites $LaFeO_3$ (LF) and $LaTi_{0.5}Mg_{0.5}O_3$ (TM (50:50)) were synthesized in the similar way. Using MCA method, perovskites were obtained in rather short time and at room temperature. The samples were characterized by X-ray powder diffraction (XRPD), X-ray photoelectron spectroscopy (XPS), scanning electron microscopy (SEM) with energy dispersive X-ray spectroscopy (EDS), temperature programmed desorption of oxygen (TPD), Mossbauer spectroscopy, BET surface area measurements and tested in methane deep oxidation. According to XRPD analysis all

synthesized samples are almost single perovskite phase, with trace amounts of La_2O_3 phase. Data of Mossbauer spectroscopy identify Fe^{3+} in octahedral coordination. The activity of perovskite in methane deep oxidation increases in the order TM (50:50) < MF series < TF series. Higher activity of TF samples in respect to MF with similar Fe content can be related to the structural characteristic, mainly to the presence of predominantly most labile oxygen species evidenced by TPD at lowest temperature of oxygen evaluation. In used experimental conditions, the Fe substituted perovskite are thermal stable up to the temperature of 850 ^{0}C. The stability of Fe active sites is probably the most important parameter responsible for thermal stability of perovskite, but the atomic surface composition also should be taken into account.

J W Seo *et al.* 2008[57] reviews the growth, structural and magnetic properties of LFO thin films as well as exchange coupling to a FM layer. Antiferromagnetic (AFM) orthoferrites are interesting model systems for exploring the correlation between their crystalline and AFM domains and the resulting exchange bias when coupled to a ferromagnetic layer. In particular, $LaFeO_3$ (LFO) has a Neel temperature, T_N = 740 K, which is the highest in the orthoferrite family. The recent developments of synchrotron radiation-based photoelectron emission microscopy (PEEM) have provided the possibility of studying AFM domain structures as well as the magnetic coupling between the AFM and the adjacent ferromagnetic (FM) layer, domain by domain. Thin films of LFO have proved excellent candidates for such studies because their AFM domains are well defined and large enough to be readily imaged by PEEM. A significant increase of the exchange bias field by a factor of about 10 was obtained when LFO was diluted with Ni atoms in the volume part. In this sample, the structural domain boundary became corrugated due to substitution defects. The results indicated the details of the precise domain boundary configuration strongly affecting the exchange coupling. The structural domain configuration in LFO can change with the substrate material, orientation and its miscut. In LFO, due to the Fe–O–Fe super exchange, which determines the AFM properties as well as the orthorhombicity of the unit cell, structural domains are directly correlated with AFM domains. Consequently, exchange bias can be modified by changing the structural domain configuration. The domain boundary configuration at the atomic scale also plays an important role to the resulting exchange bias field. In addition, a ten-fold increase of exchange bias was obtained by diluting LFO in the volume part.

E. Venkata Ramana *et al.* 2009[58] synthesized polycrystalline samples of $LaFeO_3$-$BaTiO_3$ to examine the structural and magnetic behaviour. X-ray diffraction confirmed that the ceramics had tetragonal symmetry with less tetragonal strain (c/a) than $BaTiO_3$. The magnetic hysteresis measured at room temperature suggested that the magnetic nature deviates from that of the parent $LaFeO_3$, which has antiferromagentic with a G-type spin structure. Improved magnetic behaviour of the solid solution compound might be due to the increase in the canting angle of the spin. The presence of oxygen vacancies and fluctuating Fe valence, arising from the substitution of Ba^{2+} and Ti^{4+} at the A- and B-sites of the lattice, might contribute to bulk magnetization. The temperature dependent magnetization indicated that magnetization was higher at low temperatures and showed a decreasing trend with increasing temperature to room temperature. The magnetic transition temperature of these samples was 665 K and 743 K for the mixed system and $LaFeO_3$, respectively. Single phase $(Ba_{0.5}La_{0.5})$ $(Ti_{0.5}Fe_{0.5})$ O_3 ceramic samples with a tetragonal unit cell were synthesized using a ceramic route. The addition of $BaTiO_3$ to $LaFeO_3$ resulted in a decrease in unit cell volume. The magnetic hysteresis deviated from that observed for antiferromagentic $LaFeO_3$. The resulting magnetization might be due to the canting of spin. The M-T data at low temperatures exhibited higher magnetization while a change in the magnetic state was observed at 665 K.

P. Palmisano *et al.* 2009[59] aimed at developing oven walls with self-cleaning properties, via catalytically enhanced thermal oxidation of soiling material within the standard range of household oven, temperatures, i.e. up to 300 °C. The Ozawa method was adopted to calculate the activation energy for the catalytic combustion of palmitic acid on, e.g. ceria showing a very low value of 50 kJ/mol compared to the 90 kJ/mol for the non-catalytic combustion. The prepared catalysts were then deposited on steel sheet samples coated with commercial enamel by *in situ* spray pyrolysis. The obtained catalytic layers were characterized by SEM–EDS analysis to assess their integrity and adhesion to enamel and the obtained phases. Some saturated fatty acids, e.g. myristic (tetradecanoic), palmitic (hexadecanoic) and stearic (octadecanoic) acids, were selected as single soiling compounds to investigate their thermal degradation behaviour under different operating conditions. $MnCr_2O_4$, $LaFeO_3$ and CeO_2 were chosen as oxidative catalysts and synthesized by the "Solution Combustion Synthesis" (SCS) method. The catalytic activity towards fatty acids was tested in a temperature programmed combustion (TPC) apparatus. The self-cleaning performance of the coated sample activity was measured in a standard oven, by performing a cooking cycle simulation (250 °C for 60 min; soiling by olive oil and pork lard); the weight loss and aesthetic

appearance were benchmarked versus a bare, non-catalytic enamel surface. The CeO_2 catalyst showed the best adhesion properties as well as the best performances towards the combustion of the three selected fatty acids, whereas the $MnCr_2O_4$ catalyst provided the best performance towards both the pork lard and the olive oil catalytic combustion with fat removal per cycle of about 18% and 40%, respectively.

Jing Leng *et al.* 2010[60] synthesized ultrafine one-dimensional $LaFeO_3$ nanofibers by electrospinning utilizing sol–gel precursors. The surface morphology, microstructure and crystal structure were investigated by scanning electron microscopy, X-ray diffraction and transmission electron microscopy. The nanofibers with smaller diameter were continuous and uniformly distributed. Typical fiber diameter was between 180 nm and 220 nm and the average diameter was 200 nm. The fibers consisted of many single-crystal $LaFeO_3$ grains and the grain size was about 20–50 nm. The relationship between the diameter of as-synthesized fibers and the PVP concentration of the precursor was investigated. The experimental results indicated that the PVP concentration had a great impact on the fiber size and 5.89 wt. % PVP concentrations in sol–gel precursors was advantageous to the formation of more uniform electrospun composite fibers with smaller diameter. The one-dimensional $LaFeO_3$ nanostructure may be used as a model system to further study its magnetic properties and applications in micro/nano electronic devices, gas sensors and catalysts, etc.

Haijiao Su *et al.* 2010[61] successfully synthesized nanosized $LaFeO_3$ with large specific surface area by an impregnation process, with mesoporous silica SBA-16 as hard template and corresponding metal nitrates as La and Fe resources, and the resulting $LaFeO_3$ is also characterized by thermogravimetry–differential thermal analysis (TG–DTA), X-ray diffraction (XRD), N_2 adsorption–desorptions, Brunauer Emmett Teller (BET) technique, transmission electron microscopy (TEM), X-ray photoelectron spectroscopy (XPS), UV–visible diffuse reflection spectrum (UV–Vis DRS), and surface photo voltage spectroscopy (SPS). It is found that, compared with that prepared by the conventional citrate method, the as-prepared $LaFeO_3$ with 20-50 nm particle size has remarkable large specific surface area, even still with the surface area as large as about 85 $m^2\ g^{-1}$ after calcinations at 800 ^{0}C,which is attributed to its mesoporous structure as well as the small particle size. During the photo catalytic degradation of Rhodamine B solution under visible irradiation, all the $LaFeO_3$ samples obtained are superior to P25 TiO_2, and the activity becomes high with increasing calcinations temperature. It is revealed that the excellent photo catalytic performance is

mainly ascribed to the large surface area and high photo generated charge separation rate. The study provides a new route to design and synthesize other metal composite oxides with large surface area, and would broaden the scope of the application of perovskite-type materials. The superior visible photocatalytic performance of this $LaFeO_3$ over international P25 TiO_2 is confirmed, implying that the porous perovskite-based nanomaterials, as non-TiO_2-based visible-driven photocatalysts, are feasible and promising.

Hossein Ahmadvand *et al.* 2010[62] prepared nanoparticles of antiferromagnetic $LaFeO_3$ by the sol–gel method. An exchange bias effect has been observed and is attributed to the exchange coupling between the ferromagnetic shell and antiferromagnetic core of the particles. The results provide clear evidence of the presence of spontaneous exchange bias in this system. After field cooling from room temperature, the exchange bias increases while the coercivity decreases with decreasing temperature. Taking into account the role of thermal activation, the temperature dependence of exchange bias and coercivity has been interpreted in terms of the spontaneous exchange bias mechanism proposed recently. The nanoparticles of AFM $LaFeO_3$ exhibit EB properties. This effect originates from the coupling between the FM shell and the AFM core of the particles. Thermally activated reversal of the AFM spins can explain the appearance of EB without the conventional FC, as well as the temperature dependence of EB and coercivity.

S. Acharya *et al*. 2010[63] prepared $LaFeO_3$ by solid state reaction method using Fe_2O_3 and La_2O_3 as starting materials. The crystallographic phase of the $LaFeO_3$ has been confirmed by X-ray diffractograms. Magnetic mass susceptibilities (χ_m) of the sample at different magnetic fields have been measured in the temperature range of 300–14 K. Thermal variations of χ_m and the observed ac magnetic hysteresis loop indicate the presence of magnetic ordering in $LaFeO_3$. Ferroelectric hysteresis loop observed at room temperature indicates the presence of ferroelectric ordering in $LaFeO_3$. Measured values of dielectric constant in the presence and absence of magnetic field confirmed that $LaFeO_3$ is multiferroic. Both types of spontaneous magnetization and polarization with a moderate magneto electric coupling were present in the sample. The non-linear dc magnetization along with the ac hysteresis loop confirms the presence of exchange interaction in the sample. The magneto electric coupling together with the high Neel temperature (~740 K) implies that the present $LaFeO_3$ sample would be suitable for application as multiferroic material.

Priti V. Gosavi *et al*. 2010[64] used three different wet chemistry routes, namely co-precipitation, combustion and sol–gel methods to synthesize $LaFeO_3$ perovskite with improved surface area. The synthesized perovskite was characterized by X-ray diffraction (XRD), scanning electron microscopy (SEM), energy dispersive X-ray spectrometer (EDS), Brunauer–Emmett–Teller (BET) nitrogen adsorption, ultraviolet diffused reflectance spectroscopy (UVDRS) and Fourier transform infrared (FTIR) spectroscopy techniques. Improved surface area was observed for all three methods as compared to the previously reported values. The perovskite synthesized using sol–gel method yields comparatively pure, crystalline phase of $LaFeO_3$ and relatively higher surface area of $16.5m^2\ g^{-1}$ and porosity. The material synthesized using co-precipitation method yielded other phases in addition to the targeted phase. The morphology of perovskite synthesized using co-precipitation method was uniform agglomerates. Combustion method yields flakes type morphology and that of sol–gel method was open pore type morphology. The selection of method for perovskite synthesis largely depends on the targeted application and the desired properties of perovskites. The results reported in this study are useful for establishing a simple scalable method for preparation of high surface area $LaFeO_3$ as compared to solid-oxide method. Further, the typical heating cycle followed for calcinations resulted in relatively high surface area in the case of all three methods.

Manjunath B. Bellakki *et al.* 2010[65] synthesized Ag-doped $LaFeO_3$ orthoferrites by applying a solution – based combustion process. The samples were characterized by multiple techniques to establish structure – property relationships. Specifically, for structural characterization, powder X-ray diffraction (XRD), scanning electron microscopy (SEM), energy dispersive X-ray analysis (EDX), Fourier transmission infrared spectroscopy (FTIR), Thermo-gravimetric analysis (TGA), and X-ray photoelectron microscopy (XPS) were carried out. For properties, squid magnetometer measurements (for magnetic properties), titrations (for chemical analysis), and diffuse reflectance (for optical band gap properties) measurements were carried out to elucidate structure–property relationship. Structural distortion due to Ag doping is correlated to the geometric tolerance factor t. The observed changes in magnetic properties are correlated to creation of ions of mixed valency ($Fe^{3+/}Fe^{4+}$), which increase with increasing Ag doping. The optical band gaps of the (La, Ag) FeO_3 material were determined. The mixed electronic conduction of these materials, in conjunction with favourable electronic band structure could position them for SOFC and photo catalytic applications.

Masahiro Sadakane *et al*. 2010[66] prepared three-dimensionally ordered macroporous (3DOM) lanthanum–iron-oxide ($LaFeO_3$) with different core diameters using a colloidal crystal of polymer spheres with different diameters as templates. Well-ordered 3DOM$LaFeO_3$ materials with pore sizes ranging from 127 to 321nm were obtained using a colloidal crystal template method in a high pore fraction. Ethylene glycol–methanol mixed solution of metal nitrates was infiltrated into the void of the colloidal crystal template of a monodispersed poly(methylmethacrylate) (PMMA)sphere. Heating of this PMMA–metal salt–ethylene glycol composite produced the desired well-ordered 3DOM $LaFeO_3$ with a high pore fraction, which was confirmed by powder X-ray diffraction (XRD), scanning electron microscopy(SEM), transmission electron microscopy(TEM), mercury (Hg) porosimetry, and ultraviolet–visible (UV–vis) diffuse reflectance spectra. 3DOM $LaFeO_3$ with pore diameters of 281 and 321nm shows opalescent colors because of photonics top band properties. Catalytic activity of the 3DOM $LaFeO_3$ for combustion of carbon particles was enhanced by a potassium cation, which was involved from $K_2S_2O_8$ used as a polymerization initiator.

S. M. Khetre *et al.* 2010[67] prepared orthorhombic structure perovskite $LaFeO_3$ nanocrystalline with size ~27 nm by glycine combustion method. The prepared $LaFeO_3$ nanocrystals were characterized by TG-DTA thermal analysis, X-ray diffraction (XRD), scanning electron microscopy (SEM), atomic fluorescence microscopy (AFM) and Brunauer Emmett Teller (BET) nitrogen absorption. The $LaFeO_3$ nanocrystals are more attractive in the field of catalytic application and process can be applied to prepared more other oxide nanocrystals such as $LaCrO_3$, $LaMnO_3$ etc. The obtained $LaFeO_3$ crystals with fine particle size of nanometer give a relatively high value of surface area of about 2.5 m^2/g. This method can be also applicable for other complex oxides such as $LaCrO_3$, $LaMnO_3$ and the $LaFeO_3$ nanocrystals are more attractive in the field of catalytic application and process can be applied to prepared more other oxide nanocrystals.

Tatsuo Fujii *et al.* 2011[68] synthesized nanocrystalline $LaFeO_3$ particles at low temperatures by using hot soap technique. The synthesis was based on the thermal decomposition of organometallic compounds precipitated in a hot coordinating solvent. Moderate heat treatment at low temperature far below the combustion point of organic compounds produced spherical $LaFeO_3$ nanoparticles with average diameter of about 15 nm. The crystalline phase, structure and particle size of obtained products were characterized by

X-ray diffraction, infrared spectroscopy and transmission electron microscopy observations. In spite of the antiferromagnetic nature of bulk $LaFeO_3$, the obtained nanoparticles exhibited anomalous large magnetization. Super paramagnetic behaviour with a blocking temperature of about 30 K was observed in both magnetization and Mossbauer spectroscopic analyses. With increasing the heat treatment temperature, the grain size of $LaFeO_3$ particles was increased. The $LaFeO_3$ nanoparticles prepared at 350 °C exhibited super paramagnetic behaviour and had anomalous large net magnetization. The low blocking temperature of about 30 K indicated that the obtained nanoparticles were magnetically isolated with each other.

Monica Popa *et al.* 2011[69] obtained reactive lanthanum orthoferrite nanoparticle by a polymeric precursor route. Nanoparticle growth and crystallization from amorphous precursor, as well as the formation of a grain boundary network in polycrystalline aggregates at different calcinations temperatures were studied by conventional and high-resolution electron microscopy; electron and X-ray diffraction analysis; Raman; IR; and UV–visible spectroscopy. Microstructure measurements were compared to X-ray diffraction and chemical analysis results. Electron diffraction, combined with electron microscopy results were used to determine the content of amorphous phase. The coherent crystalline domain size and the particle size have been monitored by XRD and electron microscopy in order to determine the evolution of both crystal size and the onset temperature for crystallites formation. The results demonstrate that at 550 °C we obtain pure single-phase nanocrystalline $LaFeO_3$, sized ~40 nm, without the presence of amorphous phase. The magnetization curves in the 5–350K range indicate weak ferromagnetism of the $LaFeO_3$ powders. The polymerizable complex method offers low crystallization temperature of single phase ferromagnetic $LaFeO_3$ nanopowder with a homogeneous microstructure. The carbon content in the precursor is completely eliminated by thermal treatment at 550 °C, without the formation of agglomerates or in homogeneities in grain size as the result of partial sintering. Nanopowders of $LaFeO_3$ with crystal size of 30–50nm were obtained at temperatures as low as 550 °C, without organic or carbon contamination. High-resolution electron microscopy measurements reveal that the nanopowder is composed of single crystalline grains at 550 °C. Dislocations networks and other domain boundary-related features are clearly observed after treatments at 700 and 900 °C of the highly sinterable nanopowder. Formation of grain boundaries, sintering and grain growth begins at about 700 °C. The average particle size reaches 100–120nm after successive thermal treatments at 650, 700 and 900 °C. The

magnetization vs. magnetic field curve M(H) at 5K for $LaFeO_3$ calcined at the highest temperature of 900 ˚C showed weak ferromagnetism and the non-saturation of the magnetization characteristic of antiferromagnetic ordering of the spins in the nanoparticles. Both AFM and WFM ordering can be observed in the system, influenced by the particle size and morphology.

CHAPTER- 3

EXEPERIMENTS PROCEDURE

Lanthanum ferrite, $LaFeO_3$, was prepared by high energy ball milling followed by thermal annealing. The raw materials used for the experiments were La_2O_3 (Loba Chemical) with 99.5% purity, and Fe_2O_3 (Sigma Aldrich) with 99% purity. The composition of the sample was taken according to reaction equation given below:

$$La_2O_3 + Fe_2O_3 \rightarrow 2LaFeO_3$$

The raw materials were weighed in their stoichiometric composition and then mixed manually by using pestle mortar for one hour. Further the powders were wet milled in acetone media for 3 hours using in zirconium jar using planetary ball mill. The RPM and ball to charge ratio were 150 and 2:1 respectively. After milling the excess acetone were drained and the powder were dried in normal atmosphere. The dried powder was calcined at temperatures 400^0 C, 550^0 C, 700^0 C, 800^0 C, 1000^0 C, and 1200^0C independently in muffle furnace with holding time of 4 hours with heating and cooling rate maintained at 5^0C per minute.

In another set of experiment the mixed powder were submitted to high energy ball milling in tungsten carbide jar separately for 3, 6, 9, 12, 15 and 30 hours. The RPM and ball to charge ratio was 300 and as 20:1(for 1 gram powder 20 gram ball is required) respectively. After dry milling the powders were calcined at temperatures 700^0 C, 750^0 C, and 800^0C independently with holding time of 4 hours with heating and cooling rate maintained at 5^0C per minute.

To understand the phase formation temperature the as-milled powder were studied by differential thermal analysis (DTA) and thermo gravimetric analysis technique (TGA) were carried out by using the instruments Perkin Elmer (Pyris Diamond TG/DTA). Phase identification of the annealed powders was carried out by X-ray diffraction instruments X'Pert Pro-Panlytical.

Further the powder was pressed into pellets of 10 mm diameter die under 10 ton/cm^2 pressure using hydraulic press. The pressed pellets were sintered 1000^0C temperature for two hours. For dielectric measurements the sintered pellets were coated on both sides by Ag paste. The room temperature dielectric measurements were carried out by the instruments LCR meter Agilent 4284A (frequency range 20Hz to 1MHz). The scanning electron microscopy the samples were carried out using SEM model JEOL JSEM 6510VL. Before SEM the samples were made conducting by sputtering of Ag layer of thickness 10 nm approximately. Fig. 3.1 shows the flow diagram of the processing and characterization of the samples.

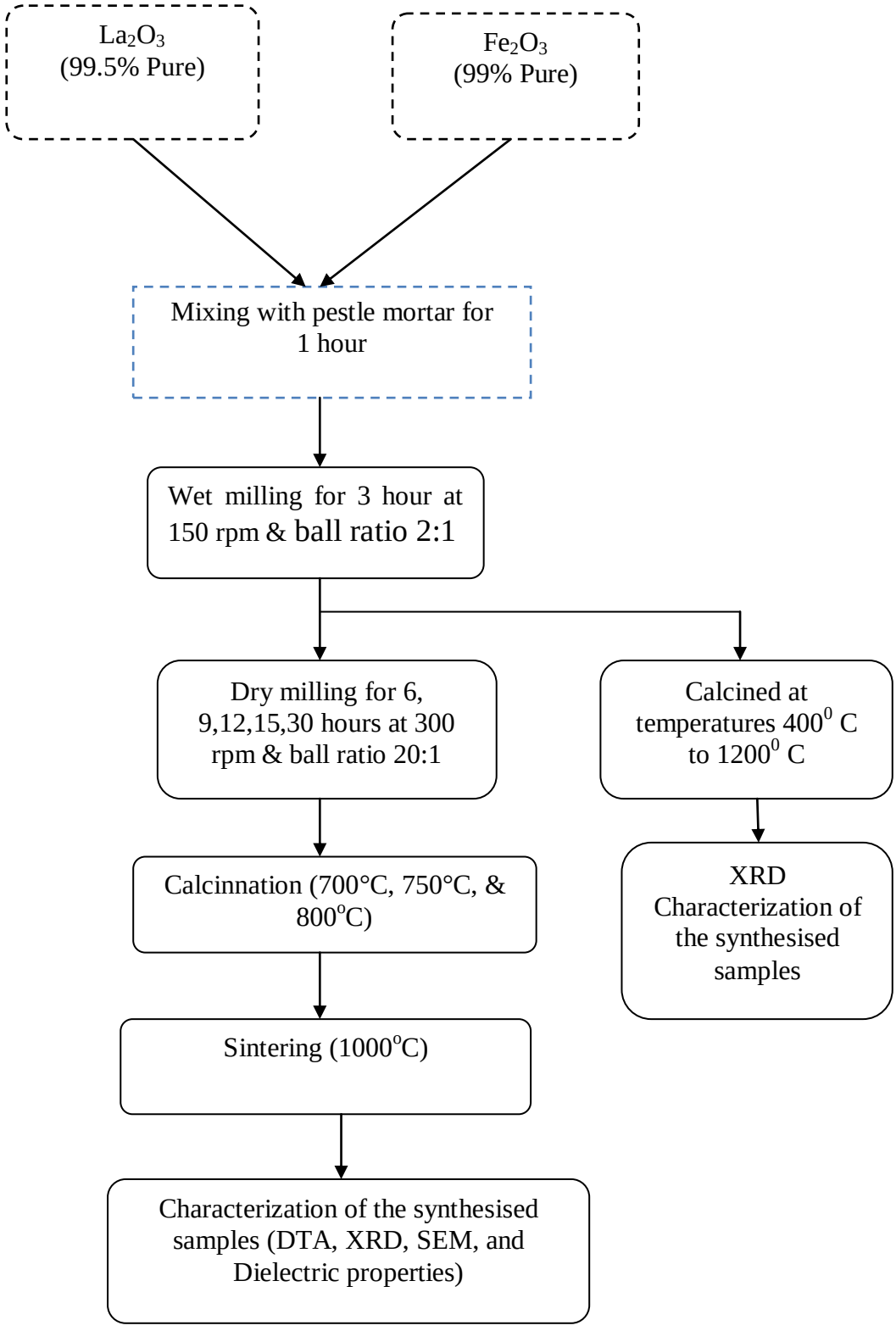

Fig. 3.1: Flow diagram

CHAPTER 4

RESULTS AND DISCUSSION

4.1 Characterization of raw materials:

Figure 4.1 (a, b) shows the X-Ray diffraction pattern of pure La_2O_3 and Fe_2O_3 respectively. It is found that both are single phase. The sample present a single phase of La_2O_3 identified as Hexagonal structure according to index card JCPDS-751900.The XRD of Fe_2O_3 show the single phase identified as rhombohedral α-Fe_2O_3 structure according to index card JCPDS-890597. The crystallite size of La_2O_3 and Fe_2O_3 calculated by Debye Scherer formula:

$$D = \frac{k\lambda}{\beta \cos\theta}$$

Where D is the crystallite size, k is the Scherer constant, λ is the wave length of radiation (λ=1.54Å), β is the peak full width at half maximum measured in radian, and θ the peak angle. The crystallite size for pure La_2O_3 is in between the range 68 nm to71nm and for pure Fe_2O_3 is 128nm.

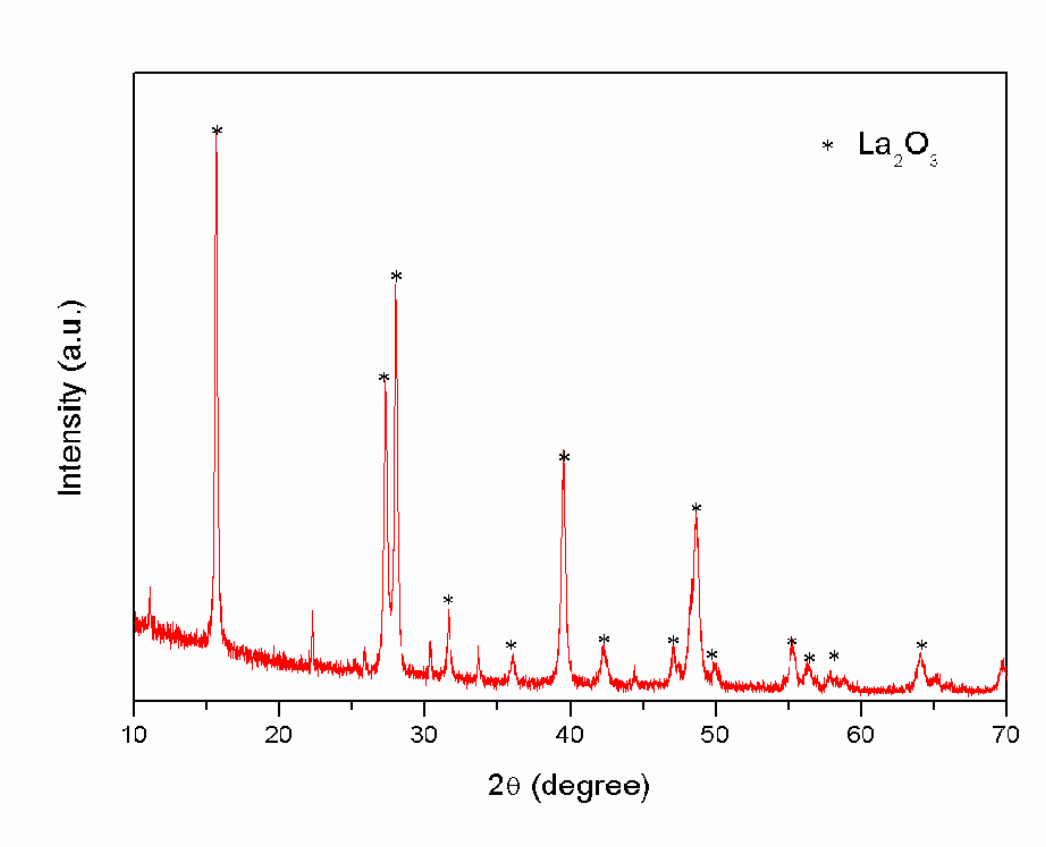

Figure 4.1(a) XRD pattern of pure La_2O_3 powder

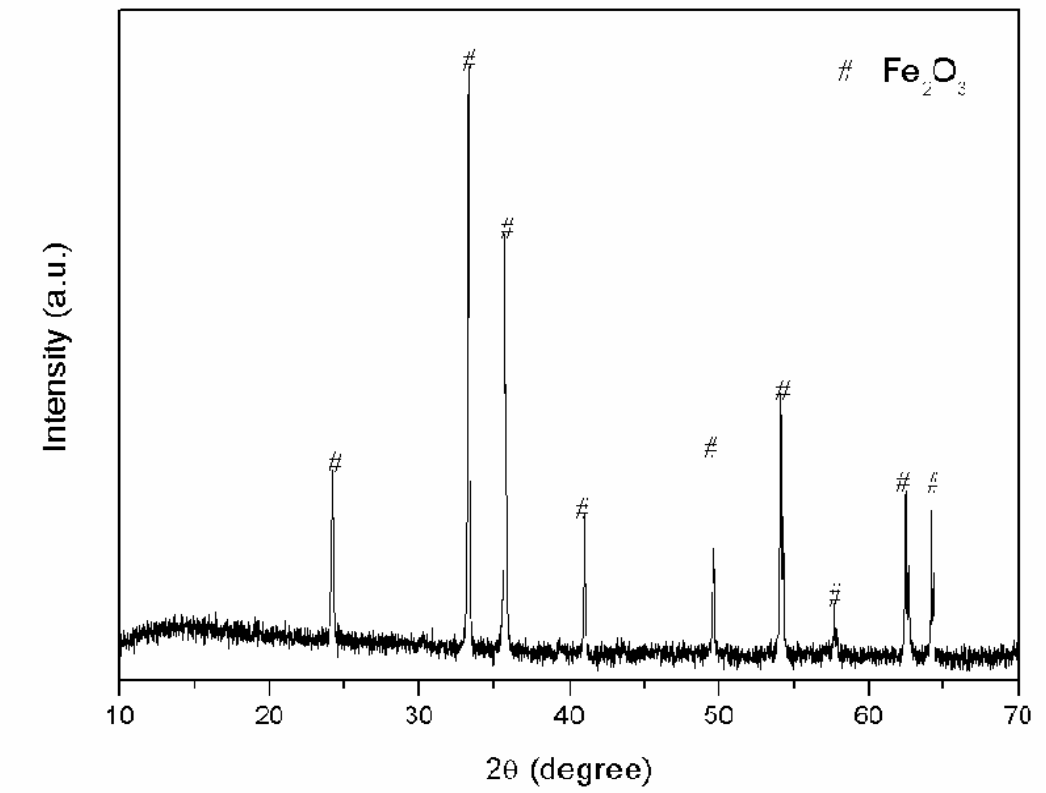

Figure 4.1(b) XRD pattern of pure Fe_2O_3 powder

4.2. Thermal Analysis

The figure 4.2 shows the DTA of mixed (La_2O_3 and Fe_2O_3) sample up to 1000 ^{0}C. The heating rate was 10 ^{0}C/minute. The DTA of the synthesis sample shows the small endothermic peaks at the temperature 344^{o}C, 495^{o}C, and 680^{o}C. The peaks at 344^{0}C and 495^{0}C arises due to intermediate phase formation. The peak at 680^{0}C corresponds to $LaFeO_3$ phase formation. This is further confirmed by X-ray studies. The corresponding TGA graph shows that in the temperature range from 0 to 300 ^{0}C the weight of the sample seems to be almost constant but as the temperature further increase above the 300 ^{0}C, then we found that drastically weight loss. Losses were continuous up to the 800^{0}C and then become constant. From above result we conclude that the $LaFeO_3$ phase formation starts at around 700^0 C.

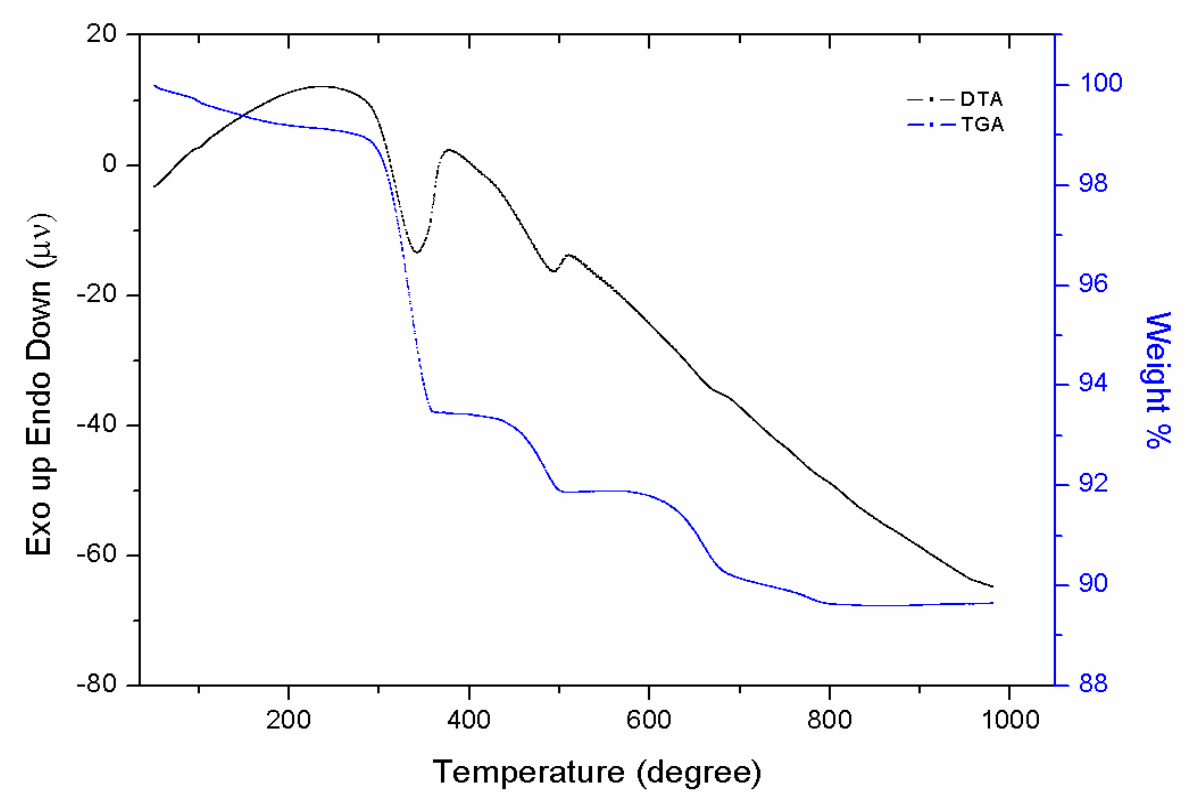

Figure 4.2: DTA/TGA curve of the milled powder (La_2O_3 +Fe_2O_3)

4.3 X-ray diffraction Studies:

Fig. 4.3 (a) shows the XRD pattern of high energy ball milled powder (Fe_2O_3 + La_2O_3) for 3 hours. It is evident that in milled sample peak broadening takes place, which indicate that particle size has been reduce. The XRD pattern of milled powder showed many peaks attributed to La_2O_3 (JCPDS 01-075-1900) and Fe_2O_3 (JCPDS 01-079-0007).

The X-ray diffraction patterns of milled powder calcined at different temperatures are shown in fig 4.3 (b-g). Samples calcined at 400^0 C to 800^0 C shows single phase are not found ,at temperature 800^0C many peaks attributed to La_2O_3 match with JCPDS card (01-083-1344) and Fe_2O_3 match with JCPDS card (01-073-2234) as the major product, together with some peaks attributed to the perovskite oxide, $LaFeO_3$, match with JCPDS card (01-088-0641) as a minor product . With increasing temperature to 1000^oC the intensity of $LaFeO_3$ (JCPDS 01-088-0641) phase increases with one impurity phase of Fe_2O_3 (JCPDS 01-073-0603) are found. Further increasing the temperature to 1200^oC Single phase $LaFO_3$ (JCPDS 01-074 2203) formed. The XRD patterns of $LaFeO_3$ calcined at temperatures above 800°C showed an increase in the intensity of the $LaFeO_3$ perovskite oxide peaks with increasing calcining temperature and a corresponding decrease in the intensity of the La_2O_3 and Fe_2O_3 peaks.

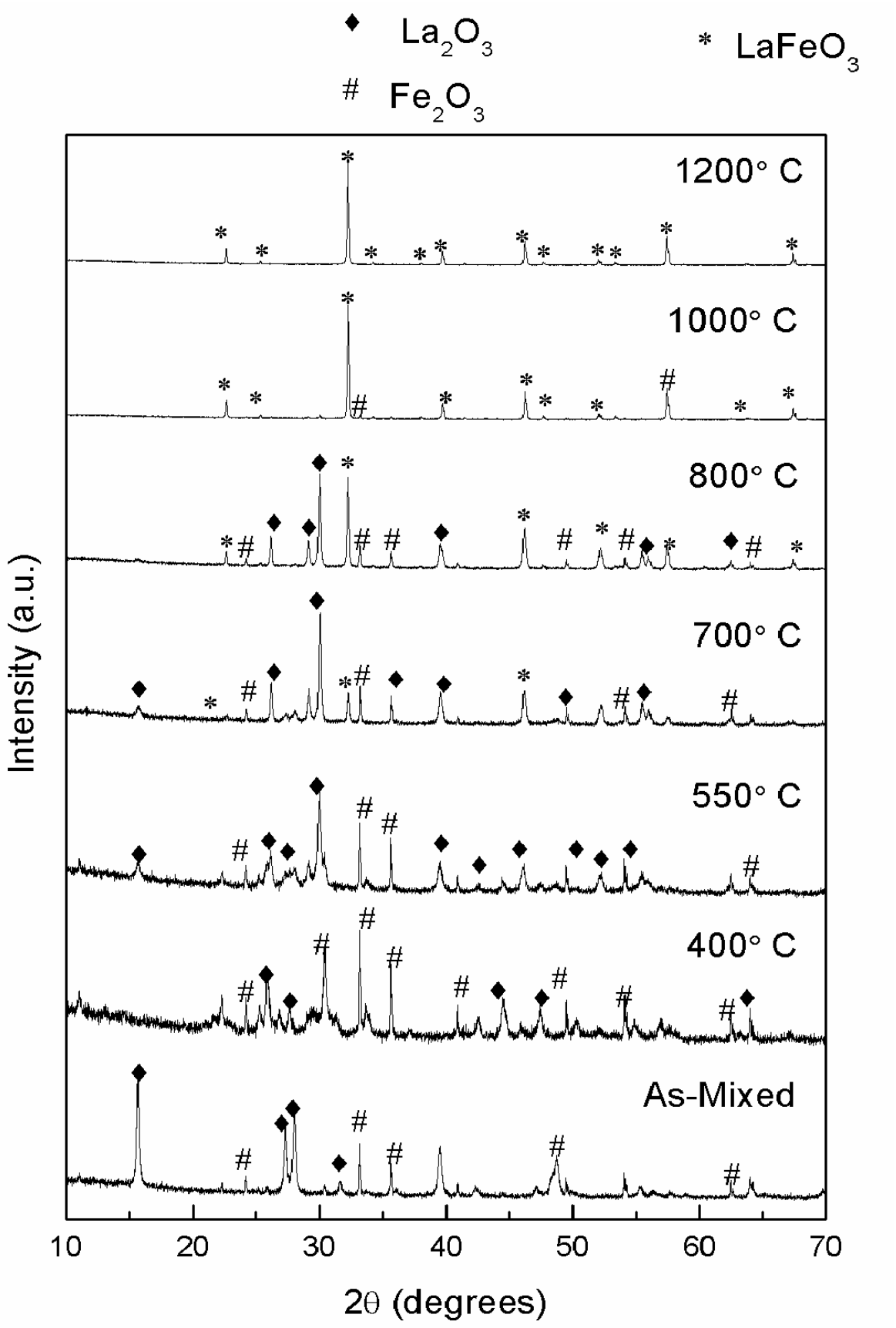

Figure 4.3 X-ray diffraction pattern (a) as mixed powder (3 hrs), (b-g) calcined powders at different temperature.

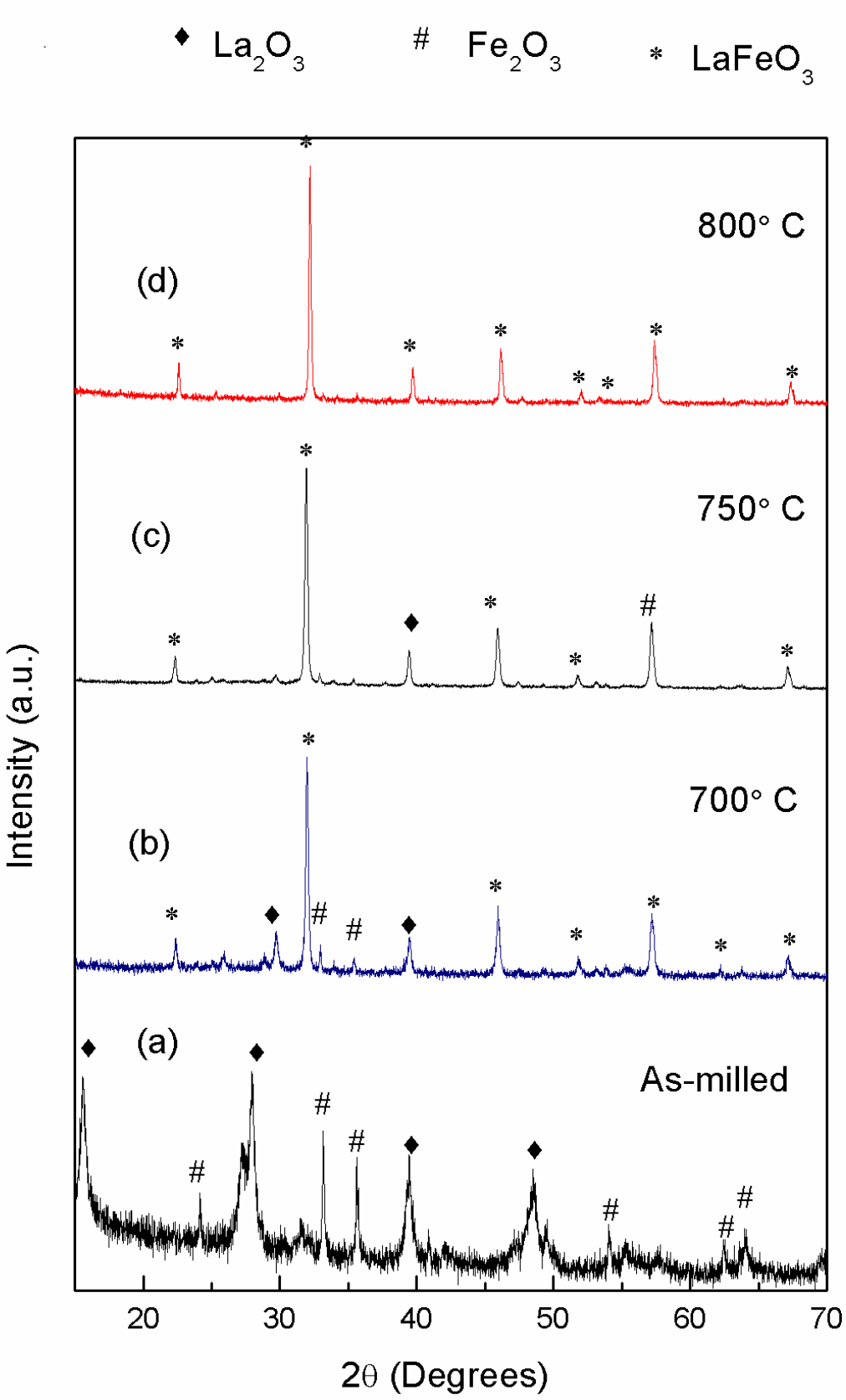

Figure 4.4 **X**-ray diffraction pattern (a) as milled powder (6 hrs), (b-d) calcined powders at different temperature

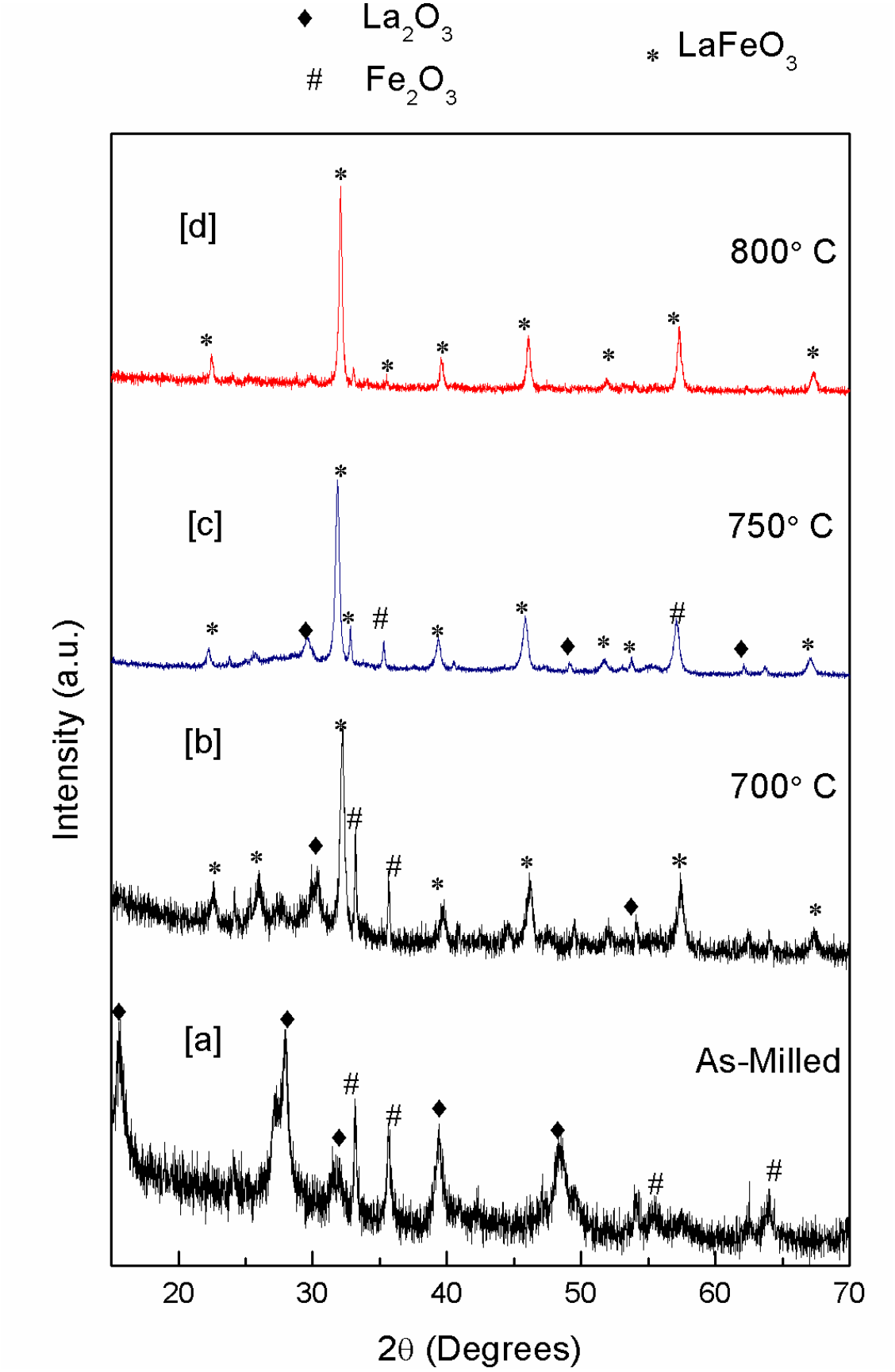

Figure 4.5 X-ray diffraction pattern (a) as milled powder (9 hrs), (b-d) calcined powders at different temperature

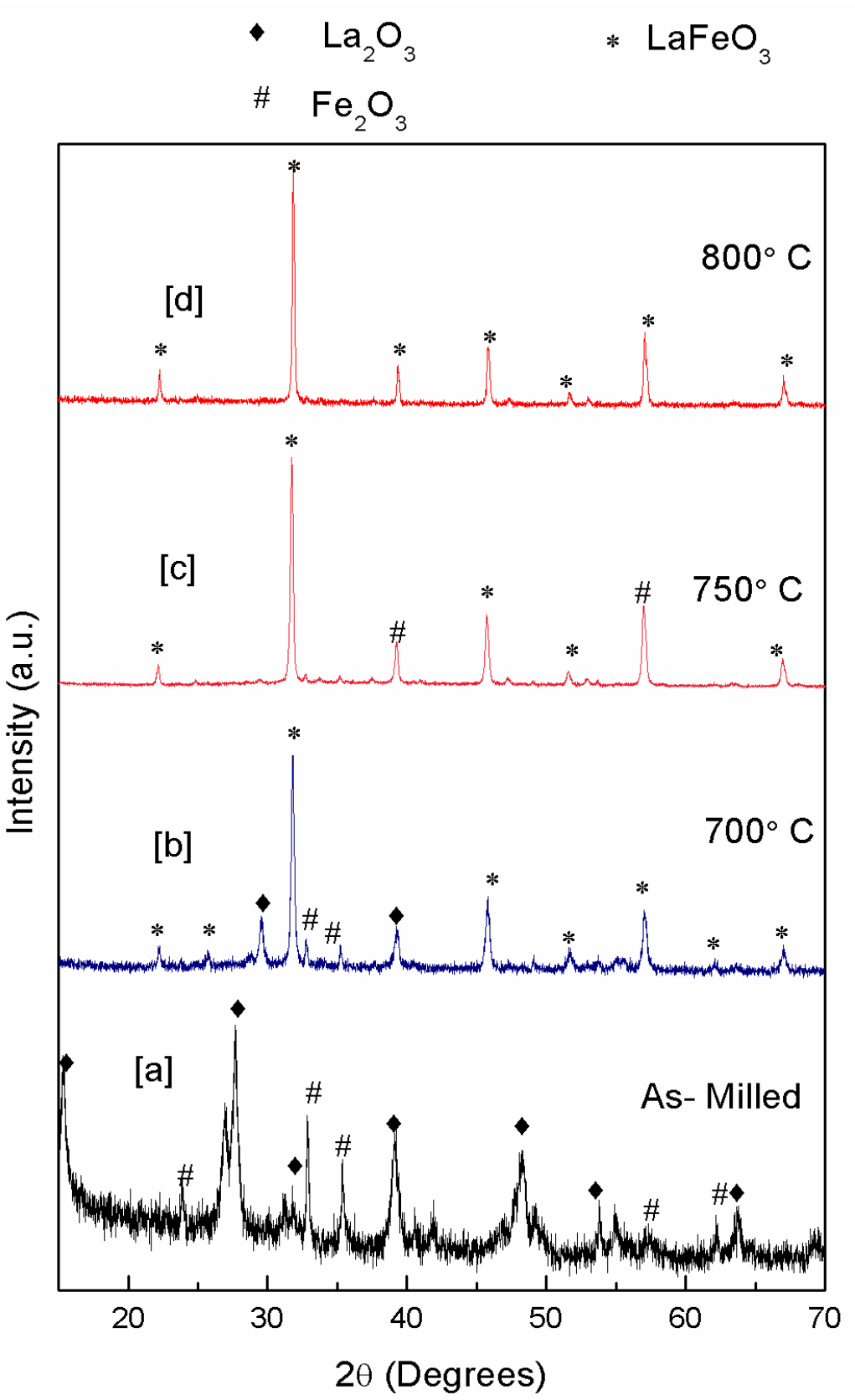

Figure 4.6 X-ray diffraction pattern (a) as milled powder (12 hrs), (b-d) calcined powders at different temperature

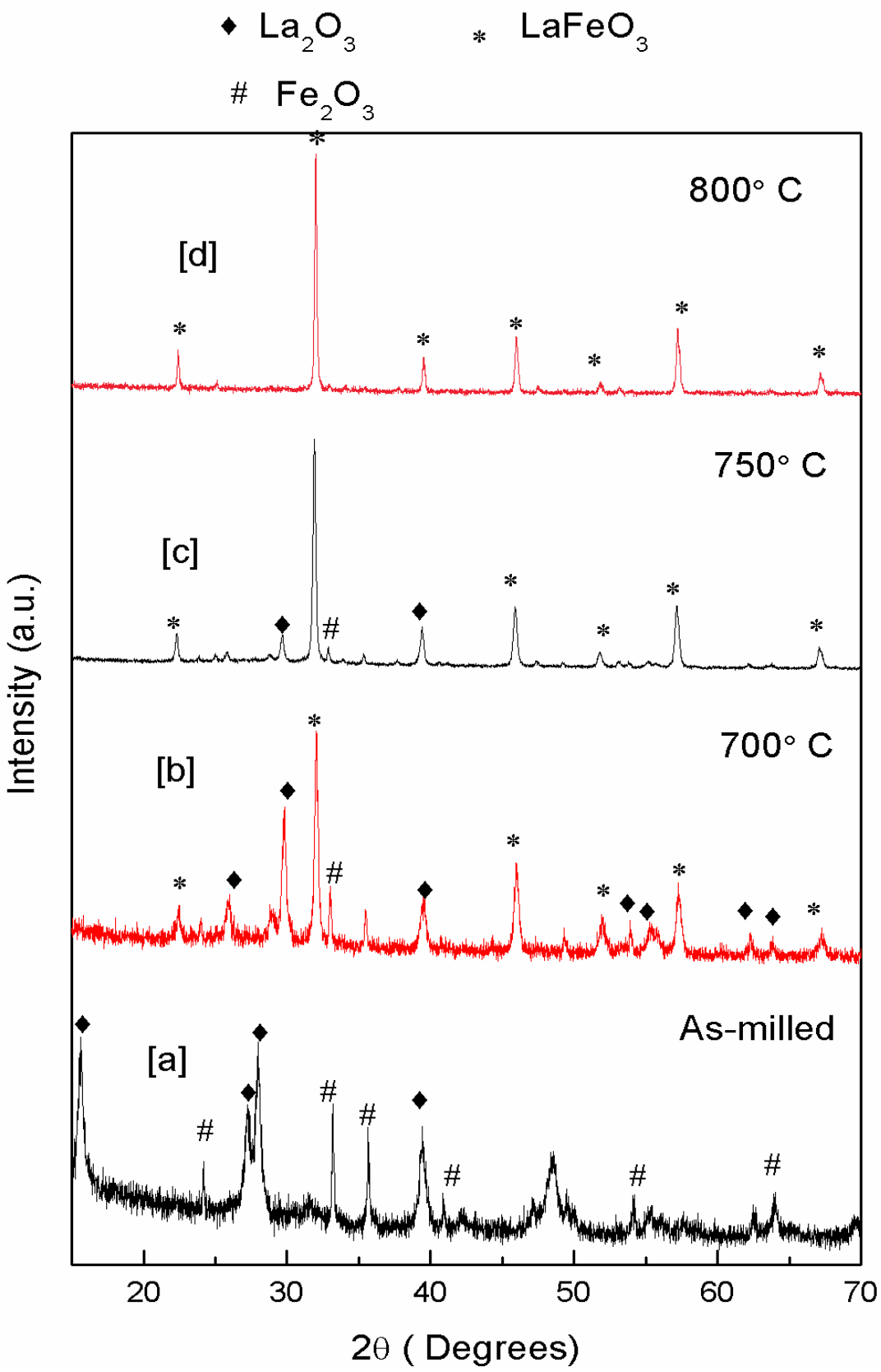

Figure 4.7 **X**-ray diffraction pattern (a) as milled powder (15 hrs), (b-d) calcined powders at different temperature.

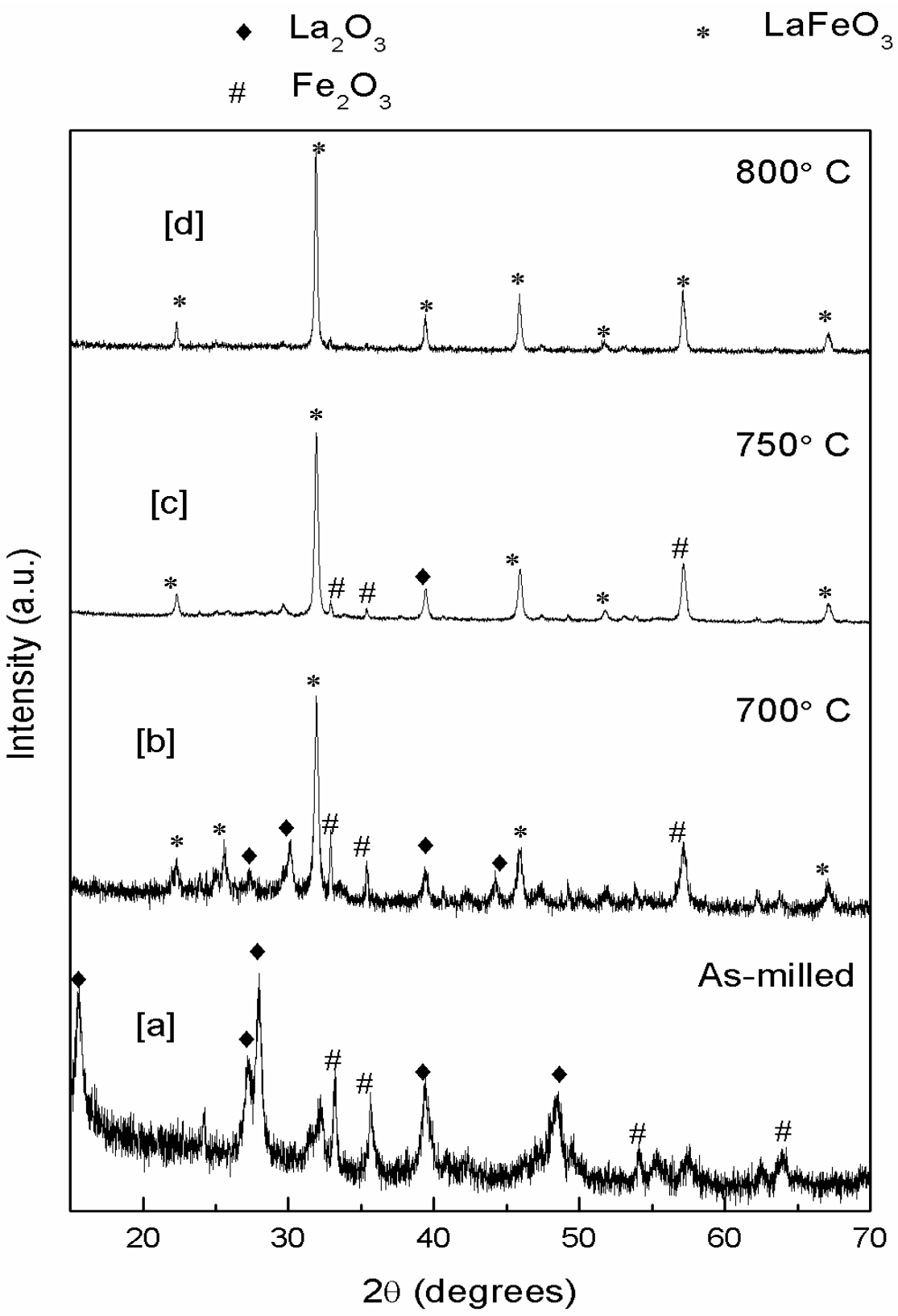

Figure 4.8: X-ray diffraction pattern (a) as milled powder (30 hrs), (b-d) calcined powders at different temperature.

Fig. 4.4 to 4.8 (a) shows the XRD pattern of high energy ball milled powder (Fe_2O_3 + La_2O_3) for 6 hours, 9 hour, 12 hour, 15 hour and 30 hour respectively. The XRD pattern of milled powder showed many peaks attributed to La_2O_3 (JCPDS 83-2034) and Fe_2O_3 (JCPDS 79-1741) as the major products. The X-ray diffraction patterns of milled powder calcined at different temperatures 700^0C, 750^0C and 800^0C are shown in fig 4.4 to 4.8, (b-d) respectively. Samples calcined at 700^0 C shows single phase are not found ,at temperature 700^0C many peaks attributed to La_2O_3 (JCPDS 83-1344) and Fe_2O_3(JCPDS 88-2359) as the major product, together with some peaks attributed , $LaFeO_3$, (JCPDS 37-1493) as a minor product . With increasing temperature to 750^oC the intensity of $LaFeO_3$ phase increases with two impurity phase of Fe_2O_3 (JCPDS 88-2359) and La_2O_3 (JCPDS 83-1344) are found. Further increasing the temperature to 800^oC Single phase $LaFO_3$ are found. And the crystallite size of $LaFeO_3$ is 73.04 nm.

The crystallite size is measured by well-known Scherer formula given earlier. The crystallite size of $LaFeO_3$ at different temperature with different milling time is given in the table 4.1. Figure 4.9 shows the variation of crystallite size with temperature. It is evident that when increase the temperature the crystal also increase with temperature.

Table 4.1 Crystallite size of $LaFeO_3$ at different temperature

Temperature (^{0} C)	**Crystallite size (nm)**				
	6 hour	9 hour	12 hour	15 hour	30 hour
700^0 C	52.78	24.25	45.69	29.87	31.19
750^0 C	46.56	31.18	61.59	46.41	43.64
800^0 C	68.28	42.05	61.42	75.37	56.04

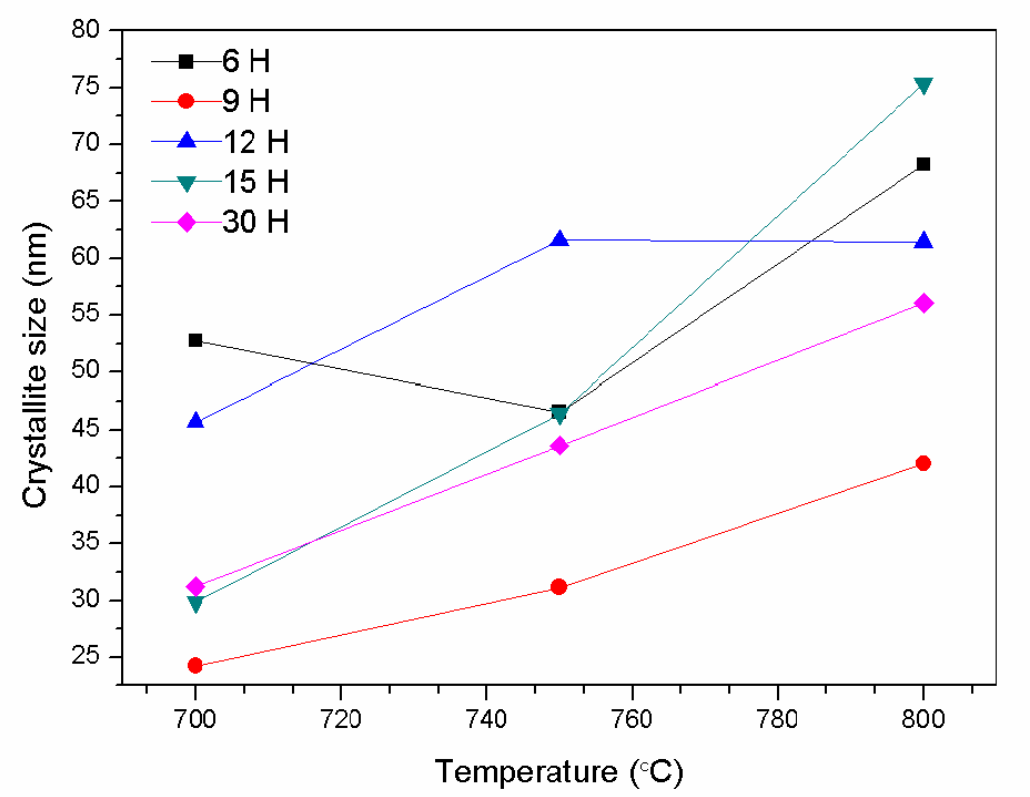

Figure 4.9 Variation in crystallite size of $LaFeO_3$ with temperature

4.4. SEM image of the pure $LaFeO_3$:

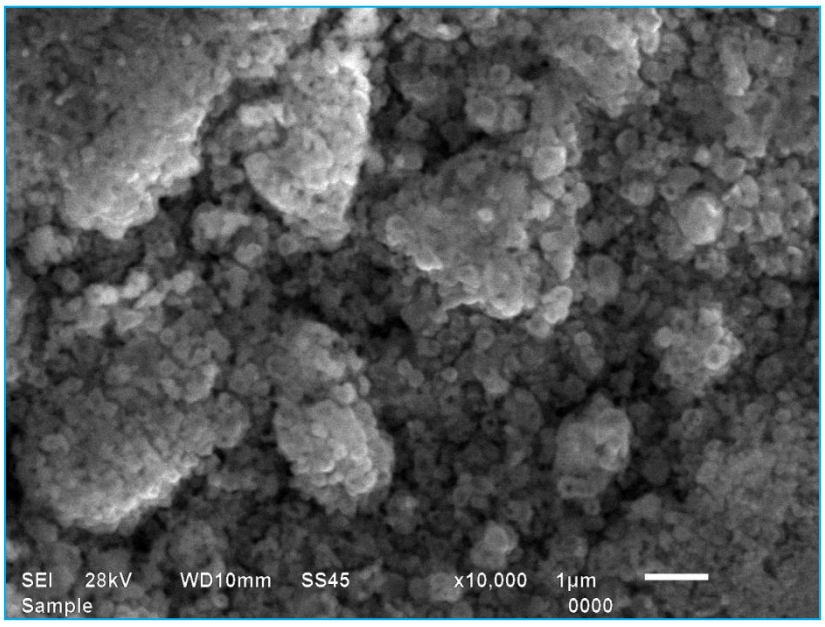

Figure 4.10: SEM of sample $LaFeO_3$ at 10,000X

Fig.4.10 shows the scanning electron micrographs of sintered pellets of $LaFeO_3$ at 10,000x magnification. The morphological study of $LaFeO_3$ pellets sintered at 1000 ^{0}C has been carried out using scanning electron microscopy. As it is clear from SEM micrograph that particles posses spherical symmetry with well uniformity. The average grain size of is found to be about 200nm. Moreover formation of clusters and aggregation also take place.

4.5. Measurements of Dielectric Properties

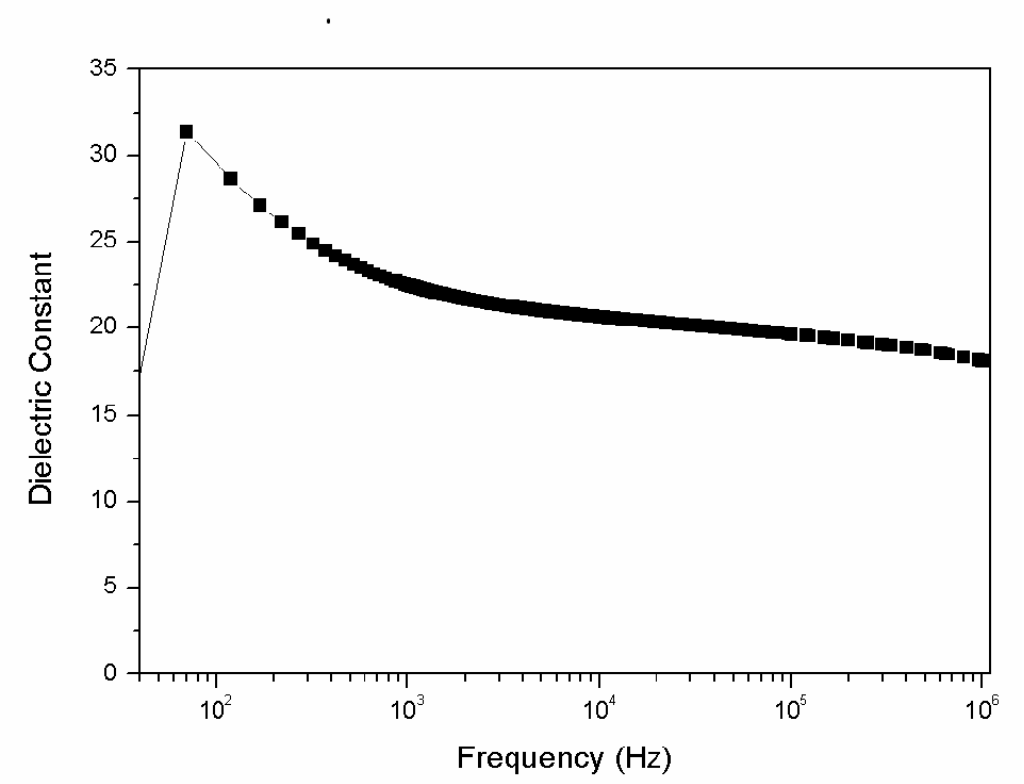

Figure 4.11: Dielectric constant in $LaFeO_3$

Fig. 4.11 shows the variation of room temperature dielectric constant measurements with respect to frequency in the range of 20Hz to 1MHz for the $LaFeO_3$ system. It was found that the value of dielectric constant was high at lower frequency and decrease as the frequency increased and become almost constant at higher frequency region. This behaviour can be understood by the dipoles relaxation phenomena where at the low frequency the dipole able to follow the frequency but at the higher frequency the dipole may have not have time to undergo relaxation.

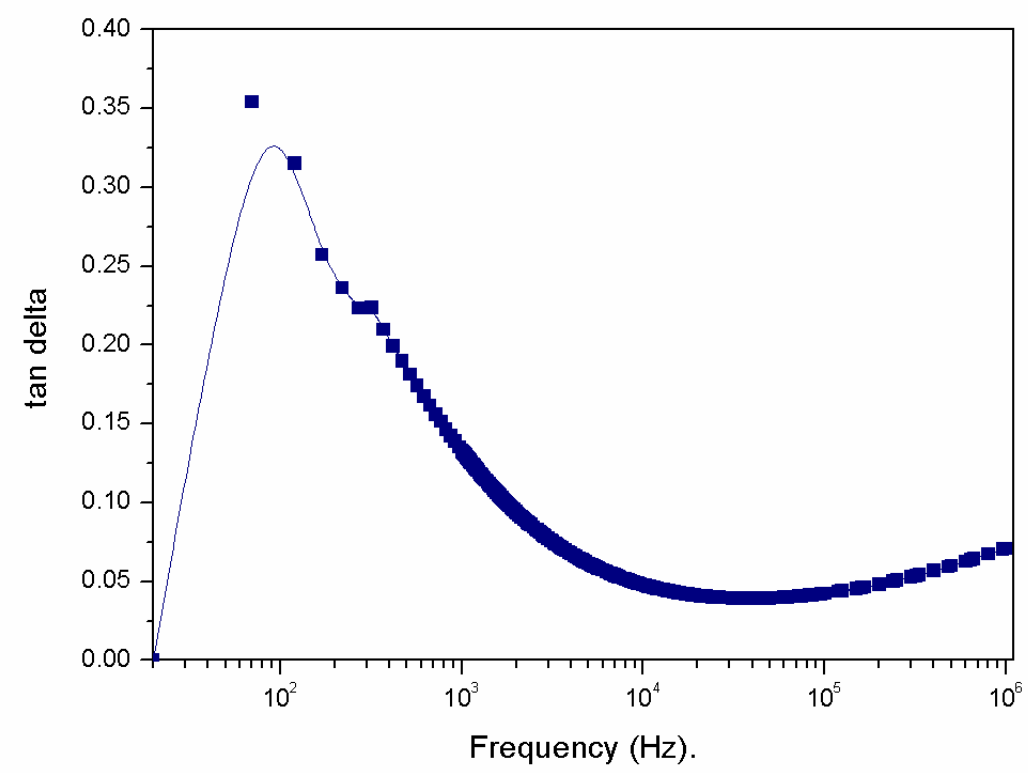

Figure 4.12: Dielectric losses in $LaFeO_3$

Fig 4.12 shows the dielectric loss with respect to frequency for $LaFeO_3$ system, at room temperature using LCR meter. It was found that loss was maximum at lower frequency but the magnitude is very low. Such system having good dielectric constant and small loss can be used for variety of applications in the field of dielectric and memory devices.

CONCLUSION

The aim of my present work is the synthesis and characterization of Lanthanum ferrite, $LaFeO_3$, has been carried out.

- The Lanthanum ferrite ($LaFeO_3$) has been prepared using high energy ball milling followed by thermal annealing.
- The thermal study (TGA/DTA) reveals that there was no loss observed after 800^0C which means formation of pure and high crystalline phase of $LaFeO_3$.
- Single phase $LaFeO_3$ was formed at 1200°C for un-milled samples, however for milled samples the phase formation was completed at 800°C.
- Crystallite size of $LaFeO_3$ was found to increase with increasing temperature.
- The room dielectric studies carried out on the pellet sintered at 1000°C. It is observed that dielectric constant decrease in increase frequency from 70 Hz to 1 Mhz. lower frequency and decrease as the frequency increased and become almost constant at higher frequency region. Dielectric loss with respect to frequency measurement clearly reveals that for $LaFeO_3$ system, the loss was maximum at lower frequency but the magnitude is very low.
- The morphological study of $LaFeO_3$ pellets sintered at 1000 ^{0}C using SEM, reveals that the particles posses spherical symmetry with well uniformity. The average grain size of is found to be about 200nm. Moreover formation of clusters and aggregation also take place.

REFERENCES

1. Bhalla, A. S.; Guo, R.; Roy, R. Mat. Res. Innovat. (2000), *4*, 3.
2. Pena, M. A.; Fierro J. L. G. Chem. Rev. *(*2001), *101*, 1981.
3. Goldschmidt, V. M. Geochemisce Verterlungsgesetze der Elemente. Norske Videnskap, Oslo, 1927.
4. Tejuca, L. G.; Fierro, J. L. G.; Tascón, J. M. D. Adv. Catal. (1989), *36*, 237.
5. Glazer, A. M. Acta Cryst. B(1972), *28*, 3384.
6. Glazer, A. M. Acta Cryst. A (1975), *31*, 756.
7. Woodward, P. M. Acta Cryst. B (1997), *53*, 44.
8. J. M. D. Coey, M. Viret; S. von Molnar, Advances in Physics, (1999), 167–293.
9. Alexandra Witze, Science News Web Edition, (2010).
10. D. Treves, J. Appl. Phys. 36, (1965), 1033–1039.
11. Y.S. Didosyan, H. Hauser, H. Wolfmayr, J. Nicolics, P. Fulmek, Sens. Actuators A 106 ,(2003)168–171.
12. S. Mathur, M. Veith, R. Rapalavicuite, H. Shen, G.F. Goya, W.L.M. Filho, T.S. Berquo Chem. Mater. 16, (2004), 1906–1913.
13. S. Mathur, H. Shen, N. Lecerf, A. Kjekshus, H. Fjellvag, G.F. Goya, Adv. Mater. 14 (2002) 1405–1409.
14. J.W. Seo, E.E. Fullerton, F. Nolting, A. Scholl, J. Fompeyrine, J.-P. Locquet,J. Phys.Condens. Matter. 20 (26) (2008) 1–10.
15. I. Hole, T. Tybell, J.K. Grepstad, I. Wærnhus, T. Grande, K. Wiik, Solid State Electronics 47 (2003) 2279–2282.
16. N.N. Toan, S. Saukko, V. Lantto, Physica B 327 (2003) 279–282.
17. K.M. Parida, K.H. Reddy, S. Martha, D.P. Das, N. Biswal, Int. J. Hydrogen Energy35 (2010) 12161
18. H. Su, L. Jing, K. Shi, C. Yao, H. Fu, J. Nanopart. Res. 12 (2010) 967.
19. D. Treves, J. Appl. Phys. 36 (1965) 1033
20. R.H. Kodama, A.E. Berkowitz, Phys. Rev. B 59 (1999) 6321
21. Y.C. Lee, A.B. Parkhomov, K.M. Krishnan, J. Appl. Phys. 107 (2010) 09E124.
22. X.W. Qi, J. Zhou, Z.X. Yue, Z.L. Gui, L.T. Li, Ceram. Ind. 29 (2003) 347.
23. A.E. Ginnakas, A.K. Ladavos, P.J. Pomonis, Appl. Catal. B: Environ. 49 (2004) 147.
24. W. Zheng, R. Liu, D. Peng, G. Meng, Mater. Lett. 43 (2000) 19.

25. M. Popa, J. Frantti, M. Kakihana, Solid State Ionics 154–155 (2002) 437.
26. H. Cui, M. Zayat, D. Levy, J. Non-Cryst. Solids 352 (2006) 3035.
27. S. Geller and F.E. Wood, Acta C'ryat. 9 (1956) 563.
28. F. Bertaut and F. Forrat. J. de Phya. 17 (1956) 129
29. M. Marezio and P.J. Dernier. Miter. Res. Bull. 6 (1071) 23.
30. W.C. Koehler and E.O. Wollan. J. Phys. C'hem. Sohda 2 (1957) 100.
31. R.L. White. J. Appl. Phys. 40 (1969) 1061.
32. Fossdal, A.; Menon, M.; Wærnhus, I.; Wiik, K.; Einarsrud, M.-A.; Grande, T. *J.*
33. Moruzzi, V. L.; Shafer, M. W. *J. Am. Ceram. Soc.* 1960, *43*, 367.
34. Z.-Q. Tian, H.-T. Yu, Z.-L. Wang, Mater. Chem. Phys. 106 (2007) 126.
35. N. Russo, D. Fino, G. Saracco, V. Specchia, Catal. Today 137 (2–4) (2008) 306.
36. J. Shu, S. Kaliaguine, Appl. Catal. B: Environ. 16 (1998) L303.
37. X. Qi, J. Zhou, Z. Yue, Z. Gui, L. Li, Ceram. Int. 29 (2003) 347.
38. Y. Wang, J. Zhu, L. Zhang, X. Yang, L. Lu, X. Wang, Mater. Lett. 60 (2006) 1767.
39. T.Peterlin-neumaier and e. Steichelet,Journal of Magnetism and Magnetic Materials 59 (1986) 351-356
40. Kuiying Li *et al.,* Materials Chemistry and Physics 60 (1999) 226-230
41. Qiwu Zhang, Fumio Saito, Journal of Materials Science **36** (2001) 2287 – 2290
42. S. Nakayama, Journal of Materials Science **36** (2001) 5643 – 5648
43. A. Delmastro *et al*., Materials Science and Engineering B79 (2001) 140–145
44. Monica Popa, Johannes Frantti, Masato Kakihana, Solid State Ionics 154– 155 (2002) 437– 445
45. M. Sivakumar *et al.,* J. Mater.Chem.,(2004),14,764–769
46. Xiwei Qi *et al*., Ceramics International 29 (2003) 347–349
47. A. Fossdal, M.-A.Einarsrud, T. Grande, Journal of the European Ceramic Society 25 (2005) 927–933
48. Ivar Wærnhus, Tor Grande, Kjell Wiik, Solid State Ionics 176 (2005) 2609 – 2616
49. M. A. Gabal *et al*., J. Mater Sci (2006) 41:7597–7603
50. G. Shabbir , A.H. Qureshi , K. Saeed , Materials Letters 60 (2006) 3706–3709
51. Yanping Wang *et al.,* Materials Letters 60 (2006) 1767–1770
52. A.D. Jadhav , A.B. Gaikwad , V. Samuel , V. Ravi, Materials Letters 61 (2007) 2030–2032
53. Defne Bayraktar *et al.,* Journal of the European Ceramic Society 27 (2007) 2455–2461

54. Xiaoping Dai, Changchun Yu, Qiong Wu, Journal of Natural Gas Chemistry 17(2008)415–418
55. L.John,Berchmans,R.Sindhu,S.Angappan,C.O. Augustin, Journal of Materials Processing Technology 207 (2008)301–306
56. **S.** Petrovic *et al.*, Applied Catalysis B: Environmental 79 (2008) 186–198
57. J W Seo *et al* J.Phys.Condens. Matter 20 (2008) 264014 (10pp)
58. E. Venkata Ramana *et al.*, Journal of Magnetics 14(3),(2009), 117-119
59. P. Palmisano,P.Faraldi ,D. Fino, N. Russo, Chemical Engineering Journal 154 (2009) 251–257
60. Jing Leng *et al.*, Materials Letters 64 (2010) 1912–1914
61. Haijiao Su *et al.*, J Nanopart Res (2010) 12:967–974
62. Hossein Ahmadvand *et al.*, J. Phys. D: Appl. Phys. 43 (2010) 245002 (5pp)
63. S.Acharya,J.Mondal,S.Ghosh,S.K. Roy,P.K.Chakrabarti,Materials Letters 64 (2010) 415–418
64. Priti,V.Gosavi,Rajesh B. Biniwale, Materials Chemistry and Physics 119 (2010) 324–329
65. Manjunath B. Bellakki, Brandon J. Kelly,V. Manivannan, Journal of Alloys and Compounds 489 (2010) 64–71
66. Masahiro Sadakane *et al*., Journal of Solid State Chemistry 183 (2010) 1365–1371
67. S.M.Khetre1,H.V. Jadhav2 and S. R. Bamane,J.Chem. (2010), 82-86
68. Tatsuo Fujii *et al.*, Materials Chemistry and Physics xxx (2011) xxx– xxx
69. Monica Popa, Jose M. Calderon Moreno, Journal of Alloys and Compounds 509 (2011) 4108–4116